

RESEARCH ARTICLE

CRISPR/Cas9 mutagenesis reveals a role for ABCB1 in gut immune responses to Vibrio diazotrophicus in sea urchin larvae

Travis J. Fleming^{1,2,*}, Catherine S. Schrankel^{1,*}, Himanshu Vyas^{1,*}, Hannah D. Rosenblatt³ and Amro Hamdoun^{1,‡}

ABSTRACT

The ABC transporter ABCB1 plays an important role in the disposition of xenobiotics. Embryos of most species express high levels of this transporter in early development as a protective mechanism, but its native substrates are not known. Here, we used larvae of the sea urchin Strongylocentrotus purpuratus to characterize the early life expression and role of Sp-ABCB1a, a homolog of ABCB1. The results indicate that while Sp-ABCB1a is initially expressed ubiquitously, it becomes enriched in the developing gut. Using optimized CRISPR/Cas9 gene editing methods to achieve high editing efficiency in the F₀ generation, we generated ABCB1a crispant embryos with significantly reduced transporter efflux activity. When infected with the opportunistic pathogen Vibrio diazotrophicus, Sp-ABCB1a crispant larvae demonstrated significantly stronger gut inflammation, immunocyte migration and cytokine Sp-IL-17 induction, as compared with infected control larvae. The results suggest an ancestral function of ABCB1 in host-microbial interactions, with implications for the survival of invertebrate larvae in the marine microbial environment.

KEY WORDS: CRISPR/Cas9, ABC transporter, ABCB1, IL-17, Gut epithelial immunity, Vibrio, Sea urchin, Gastrulation, Marine larvae

INTRODUCTION

Successful development depends on the precise regulation of small molecule movement across cell membranes. This is especially important for free-living 'orphan' embryos and larvae, which lack systemic circulation or specialized organs for xenobiotic metabolism, vet develop in direct contact with bioactive small molecules in their environment (Bard, 2000; Hamdoun and Epel, 2007). The marine ecosystem is particularly rich in these compounds, which are produced by diverse marine phytoplankton and bacteria (Turner and Tester, 1997; Pohnert et al., 2002; Adolph, 2004; Steele et al., 2011; Calle, 2017). How planktonic organisms adapt to these microbial small molecules is important to understand in light of rapid environmental change (Walworth et al., 2020).

An ancient and conserved suite of small molecule transporters (SMTs) are known to act as master regulators of small-molecule signaling and protection (Bard, 2000; Dean and Annilo, 2005;

¹Center for Marine Biotechnology and Biomedicine, Scripps Institution of Oceanography, University of California San Diego, La Jolla, CA 92093, USA. ²Program in Biological and Biomedical Sciences, Harvard Medical School, Boston, MA 02115, USA. ³Department of Developmental Biology, Stanford University, Stanford, CA 94305, USA

2568-048X

D T.J.F., 0000-0003-0993-4152; C.S.S., 0000-0002-7970-9113; A.H., 0000-0003-

Nigam, 2015; Rosenthal et al., 2019). These include the ATP-binding cassette (ABC) transporters, which handle a variety of substrates. One ABC transporter of interest is ABCB1 [aka P-glycoprotein (P-gp), encoded by MDR1]. ABCB1 was first described for its role in multiple drug resistance in cell lines (Danø, 1973; Juliano and Ling, 1976; Gros et al., 1986). ABCB1 is a plasma membrane transporter, with broad substrate specificity, thus functioning to eliminate a diverse range of hydrophobic endobiotics and xenobiotics (Szakács et al., 2006; Aller et al., 2009).

Homologs of ABCB1 are expressed in embryos and larvae of many species including zebrafish (Fischer et al., 2013), zebra mussels (Faria et al., 2010), oysters (Shi et al., 2015), water fleas (Campos et al., 2014) and sea urchins (Shipp and Hamdoun, 2012). While this protein has been demonstrated to protect early embryos against anthropogenic toxicants (Bošnjak et al., 2009; Fischer et al., 2013; Hamdoun et al., 2004), its natural substrates are not well established. Uncovering these endogenous ligands is important for understanding the evolution of this protein.

In the marine environment, a major source of bioactive small molecules is derived from bacteria that can be commensal, symbiotic or pathogenic to their animal hosts (Piel, 2009; Wilson et al., 2014; Calle, 2017; Smith et al., 2018). A number of prior observations support the hypothesis that ABCB1 may play an important protective role in host-microbe interactions in marine animals. Marine bacteria produce brominated compounds that are structurally similar to anthropogenic pollutant congeners known to bind mammalian ABCB1 (Teuten, 2005; Agarwal et al., 2014; Nicklisch et al., 2016; Le et al., 2020). Early embryos of the marine worm Urechis caupo, which develop in sediments rich in bacteria and metabolic byproducts, express higher levels of ABCB1 than those found in drug-resistant cancer cell lines (Toomey and Epel, 1993; Toomey et al., 1996). In later life stages of marine invertebrates, the intestinal epithelium becomes the tissue most exposed to microbial products (McFall-Ngai, 2002; McFall-Ngai et al., 2013). However, the function of ABC transporters remains underexplored in this context.

The goal of this study was to investigate the role of ABCB1 in host-microbe interactions in larvae of the purple sea urchin (Strongylocentrotus purpuratus). The sea urchin homolog of ABCB1/P-gp, Sp-ABCB1a, is an apically localized transporter that is expressed at relatively high levels throughout development (Gökirmak et al., 2012; Shipp and Hamdoun, 2012). In the early embryo, Sp-ABCB1a can reduce the accumulation of cytotoxic small molecules such as vinblastine (Hamdoun et al., 2004). The role of Sp-ABCB1a against endogenous marine or microbial-derived substrates in larvae is unknown.

Strongylocentrotus purpuratus larvae develop guts that contain three distinct functional compartments by 72 h post-fertilization (hpf) (Annunziata et al., 2019). Larvae can begin feeding at 3 days post-fertilization (dpf). Exposure to opportunistic pathogens, such as Vibrio diazotrophicus, causes robust and reproducible gut

^{*}These authors contributed equally to this work

[‡]Author for correspondence (ahamdoun@ucsd.edu)

inflammation (Ho et al., 2016). During the course of infection, immunocytes called pigment cells migrate to the inflamed gut, and coordinated molecular responses occur across the animal. This exposure assay has been adapted to model several aspects of host—microbe interactions (Buckley et al., 2017; Schuh et al., 2020). Importantly, transcript levels of *ABCB1* increase in *Vibrio*-exposed larvae (Buckley et al., 2017; Ho et al., 2016), suggesting that this protein may be important for host defenses.

Here, we targeted Sp-ABCB1a by optimized CRISPR/Cas9 mutagenesis and challenged larvae with V. diazotrophicus. Notably, ABCB1 transporter knockouts in other animals do not exhibit obvious morphological phenotypes unless challenged with drugs or other toxicants (Schinkel et al., 1994). Therefore, we developed a methodology to first screen for the effectiveness of synthetic single guide RNAs (sgRNAs) to Sp-ABCB1a in the F₀ generation (referred to as crispants), using bioinformatic tools and live-animal transporter substrate assays. We next exposed validated crispants to V. diazotrophicus, and found that crispant larvae exhibit significantly higher levels of inflammation than infected wild-type larvae. Our results shed light on potential bacterial substrates of ABCB1 and support an ancestral role for transporters in hostpathogen interactions. This work suggest that ABCB1 may have important implications for the adaptation of marine invertebrate larvae to changing microbial environments.

MATERIALS AND METHODS

Animals and culturing

Purple sea urchins, *Strongylocentrotus purpuratus* (Stimpson 1857), were collected off the coast of San Diego, CA, USA, and kept at 14°C in flow-through seawater tanks. Sea urchin embryos were reared in 0.22 μm-filtered local sea-water (FSW) as previously described (Hamdoun et al., 2004). For larval-stage experiments, cultures were diluted to 3–5 larvae ml⁻¹ FSW at 3 dpf and cultured in suspension with stirring paddles rotating at 15 rpm. Starting at 5 dpf, larvae were fed *Rhodomonas lens* at 3000 algal cells ml⁻¹ every 2 days.

Probe generation and whole-mount in situ hybridization

Primers used to amplify whole-mount *in situ* hybridization probe cDNAs are listed in Table S1. Primer pairs contain a T7 promoter site incorporated into either the forward (for sense probe transcription) or reverse primer (for antisense probe transcription). A probe template of ~1.4 kb was amplified from ABC transporter plasmids with the full-length coding sequence of *Sp-ABCB1a* (GenBank ID JQ390048; Addgene ID: 34939; Gökirmak et al., 2012) using Phusion high-fidelity DNA polymerase (NEB, Ipswich, MA, USA) and purified by PCR-column purification (Qiagen, Germantown, MD, USA). RNA antisense probes were transcribed with T7 synthesis and digoxigenin (DIG) labeling kits (Roche, Indianapolis, IN, USA) according to

manufacturer protocols. Our Sp-ABCB1a probe spans coding sequence in exons 2–12, starting 15 nucleotides downstream from the first translated ATG.

Whole-mount *in situ* hybridization was performed as previously described (Shipp and Hamdoun, 2012) with minor modifications. Briefly, embryos were hybridized in hybridization buffer [50% formamide, $5\times$ saline-sodium citrate (SSC), 5 mmol l⁻¹ EDTA, 0.1% Tween-20, $2\times$ Denhardt's solution, $50~\mu g~ml^{-1}$ heparin, $500~\mu g~ml^{-1}$ yeast tRNA] overnight at $62^{\circ}C$, at a final probe concentration of 0.5–1 ng μl^{-1} . Samples were washed and then incubated with anti-DIG-AP antibody (Roche, Indianapolis, IN, USA) overnight at $4^{\circ}C$ for alkaline phosphatase staining the following day. Stained samples were imaged on an AxioImager M2 microscope (Zeiss) using a $20\times$, 0.9~NA objective and color camera.

Synthetic sgRNA design and microinjection

Target sites were identified in sea urchin transporters using a commercial CRISPR design tool (Synthego, Redwood City, CA, USA) with the *S. purpuratus* reference genome (v3.1.38). In order to maximize the likelihood of disrupting the encoded protein, sites were selected to target an N-terminal region of coding sequence or the nucleotide binding domain (NBD) of each transporter, which are required for ATP-driven active transport. The four target sites were checked for potential off-target sites by performing BLAST analysis against the sea urchin genome. The *Sp-nodal* sgRNA was synthesized from published sequence (Lin and Su, 2016). For enhanced stability, all sgRNAs were synthesized with 2′-*O*-methyl 3′ phosphorothioate modifications in the first and last three nucleotides (Hendel et al., 2015). All sgRNAs were synthesized by Synthego (Table 1): 1.5 nmol of each sgRNA was resuspended in 15 μl nuclease-free water and stored in aliquots at −80°C.

Cas9 mRNA was synthesized from a *Streptococcus pyogenes* pCS2-nCas9n plasmid with the Thermo Fisher mMESSAGE mMACHINE SP6 Transcription Kit according to the manufacturer's protocol. pCS2-nCas9n was a gift from Wenbiao Chen (Jao et al., 2013) (Addgene plasmid 47929, RRID:Addgene_47929). For microinjections of one-cell sea urchin embryos, each sgRNA was mixed with capped nls-Cas9-nls mRNA at final concentrations of 150 and 750 ng μ l⁻¹, respectively. These were the optimal concentrations as determined by Lin and Su (2016).

Sp-ABCB1a MASO design and morphant analysis

An ATG-blocking Sp-ABCB1a morpholino antisense oligonucleotide (MASO) was designed in the 5' UTR region of Sp-ABCB1a, 33 base pairs upstream of the translation start site (Table S1). The Sp-ABCB1a MASO and a negative control MASO (Table S1) were microinjected into one-cell sea urchin embryos at a concentration of 125 ng μ l⁻¹.

Table 1. CRISPR target sites and synthetic sgRNA sequences

Gene name	Target site with PAM (5′–3′)	Synthetic sgRNA
Sp-nodal sgRNA E1-157	CGTCCGGTGTGATAAGAGG	CGUCCGGUGUGAUAAG
Sp-ABCB1a sgRNA E12-23	TCCGTGACCTCAACGTGAGCTGG	UCCGUGACCUCAACGUGAGC
Sp-ABCB1a sgRNA E12-82	ATCGTGGTCGCAAACAGGATCGG	AUCGUGGUCGCAAACAGGAU
Sp-ABCB1a sgRNA E13-22	GAGCGAGGAGCTCAGCTGTCCGG	GAGCGAGGAGCUCAGCUGUC
Sp-ABCB1a sgRNA E13-128	AGCCTCACTCTCGGTGTCCAGGG	AGCCUCACUCUCGGUGUCCA
Sp-ABCB1b sgRNA E2-158	GCCACTGCCGCCATCACTACCGG	GCCACUGCCGCCAUCACUAC
Sp-ABCB1b sgRNA E2-273	CTGCAGTCAACCGAGAAGAATGG	CUGCAGUCAACCGAGAAGAA
Sp-ABCB1b sgRNA E4-33	CCGCTACAGCACCCAAGACGAGG	CCGCUACAGCACCCAAGACG
Sp-ABCB1b sgRNA E4-170	TAACGTTCTTGTAGTGTGCATGG	UAACGUUCUUGUAGUGUGCA

sgRNA, single guide RNA; PAM, protospacer adjacent motif (underlined in each sequence).

Genomic DNA extraction and PCR

To determine Cas9 cutting efficiency, genomic DNA (gDNA) was extracted from control (wild-type, WT) and injected embryos at 48 hpf. Briefly, 50–100 embryos were pipetted into 100 µl of homogenization buffer (100 mmol l⁻¹ Tris-Cl pH 8.5, 200 mmol l⁻¹ NaCl, 0.2% SDS, 5 mmol l⁻¹ EDTA, 100 μg ml⁻¹ proteinase K) and incubated at 55°C for 2 h. Proteinase K was heat inactivated at 95°C for 10 min before the addition of 1 µl of RNase A (10 µg ml⁻¹) and incubating at 37°C for 30 min. Samples were then mixed 1:1 with a phenol:chloroform: isoamyl alcohol (25:24:1) solution, mixed, vortexed and centrifuged to phase separate gDNA in the aqueous phase. The extraction was repeated once and then the aqueous phase was precipitated overnight in 1/10th volume of 3 mol 1^{-1} sodium acetate solution (pH 5.2) and 2.5 volumes of 100% ethanol. Following overnight precipitation, gDNA was centrifuged, washed once with 70% ethanol, resuspended in nuclease-free water and stored at -20° C until use. Target regions were amplified using PrimeSTAR® Max DNA Polymerase (Takara Bio USA, Mountain View, CA, USA) and gene-specific primers (Table S1). In preparation for Sanger sequencing, PCR amplicons were re-amplified with M13-tailed primers (Table S1).

T7 endonuclease I assay of CRISPR-induced genomic mutations

T7 Endonuclease I (NEB) was used to detect the genomic mutations created by CRISPR/Cas9 mutagenesis as per the manufacturer's protocol, with minor modifications. Briefly, 500 ng of PCR-amplified genomic fragments were denatured and re-annealed in T7E1 buffer (50 mmol l^{-1} NaCl, 10 mmol l^{-1} Tris-HCl, 10 mmol l^{-1} MgCl₂, 1 mmol l^{-1} DTT, pH 7.9 at 25°C) at a total reaction volume of 19.5 μl , and incubated with 5 U of T7E1 for 25 min at 37°C. The enzymatic reaction was terminated using 1.5 μl 0.25 mol l^{-1} EDTA and run on a 2% agarose gel to resolve the cleaved products. T7E1 negative reactions included the same quantity of re-annealed PCR amplicons and underwent the same protocol but without addition of the enzyme. PCR primers are listed in Table S1.

Inference of CRISPR Edits analysis of mutation frequency

PCR-amplified fragments encompassing sgRNA target sites in both controls and crispants were Sanger sequenced using M13 sequencing primers (Eurofins Genomics, Louisville, KY, USA; Table S1). Raw sequencing (.ab1) files were analyzed using Synthego's Inference of CRISPR Edits (ICE), a commercial bioinformatic tool, similar to TIDE (Tracking of Indels by DEcomposition), that analyzes the discordance between WT and crispant sequences near the sgRNA target site (Hsiau et al., 2019 preprint). ICE predicts the Cas9 cutting efficiency and mutant alleles present in genetically modified samples.

Assays of ABCB1 efflux transport activity

ABC transporter activity was assessed by efflux assays using fluorescent substrates and inhibitors as previously described (Gökirmak et al., 2012). PSC833, calcein-AM (CAM) and Bodipy-Verapamil (Bver) were purchased from Sigma-Aldrich (St Louis, MO, USA), Biotium (Fremont, CA, USA) and Invitrogen (Waltham, MA, USA), respectively. All substrates and inhibitors were rehydrated in dimethyl sulfoxide (DMSO) and stored at -20°C. All stocks were diluted such that the final DMSO concentration did not exceed 0.5%.

Activity of transporters was assessed in sea urchin embryos at the late gastrula stage, approximately 48 hpf, or early larval stage (72 hpf). Injected crispants/morphants and un-injected embryos were incubated with CAM and Bver at final concentrations of 250 and 50 nmol l⁻¹, respectively, in FSW at 14°C for 60 min. Embryos

incubated with Bver were washed 3 times with FSW after incubation, to remove Bver remaining in the water, and immediately imaged. For inhibitor assays, embryos were incubated in 1 µmol 1⁻¹ PSC833 along with substrates. Embryos were imaged on a Zeiss LSM 700 confocal microscope using a 20× Plan-Apo, 0.8 NA air objective. All embryos exposed to the same substrate were imaged with identical confocal settings (pinhole size, gain, laser power, zoom and scan speed).

Average intracellular fluorescence intensity was measured using Fiji (Schindelin et al., 2012). For each treatment, at least 10 embryos per injection were imaged from at least three independent batches of embryos. Within each batch, fluorescence intensity was measured for WT, 1 μ mol l $^{-1}$ PSC833-inhibited and Cas9/sgRNA-injected or morpholino-injected embryos. Incubation with 1 μmol 1⁻¹ PSC833 inhibits most ABCB1-like efflux activity (Hamdoun et al., 2004); therefore, fluorescence intensity of WT and crispant embryos was compared with that of PCS833 inhibited embryos. Raw fluorescence intensity values of each individual crispant or WT embryo were divided by the mean of the raw intensity values of the PSC833-inhibited embryos to calculate the percentage substrate accumulation relative to inhibited controls. Then, the percentage substrate accumulation of each individual crispant was divided by the mean percentage substrate accumulation of the WT embryos to calculate fold-changes in accumulation.

To quantify SpABCB1a's contribution to substrate efflux, the mean fluorescence intensity of WT embryos was subtracted from all raw fluorescence intensity values of SpABCB1a crispants and PSC833-inhibited embryos. The relative contribution of SpABCB1a in CAM and Bver efflux was then calculated by comparing the fluorescence intensity of crispants with that of the PSC833-inhibited embryos.

Microbial challenge assay

To test the effects of targeted mutagenesis of *Sp-ABCB1a* on larval gut physiology and immune responses, 10 dpf *Sp-ABCB1a* sgRNA E13-22 crispants and sibling-matched control (WT) larvae were exposed to *Vibrio diazotrophicus* (Guerinot et al., 1982). Efficient ABCB1a CRISPR was validated by T7E1 and CAM efflux assays in all batches before proceeding with microbial challenges. *Vibrio* cultures were grown overnight to log phase in Marine Broth 2216 (Difco, BD Sciences) at 15°C, 250 rpm. Bacteria were washed 3 times in FSW and counted in a Petroff–Hauser counting chamber. Larvae were exposed to 10⁷ ml⁻¹ *Vibrio* in FSW or control FSW alone, as in Ho et al. (2016).

At 24 and 48 hours post-exposure (hpe), a subset of treated larvae was randomly chosen for analysis from master cultures of n>200larvae. Larvae were immobilized under a coverslip anchored with double-sided tape (0.1 mm thick, Scotch 665, 3M, Maplewood, MN, USA). Larvae were imaged on an inverted Zeiss LSM 700 using a 20× Plan-Apo 0.8 NA air objective, and scored for pigment cell migration as in Ho et al. (2016), and midgut (stomach) epithelial phenotypes as in Schuh et al. (2020). Briefly, any pigment cell that had completely emerged out of the epithelium, was in transit through the blastocoel or was localized at the gut was scored as migratory. Midgut epithelial diameters were measured in Fiji (Schindelin et al., 2012) in a Z-slice where the largest midgut cross-section was in sharp focus. The mean number of migrated pigment cells and gut epithelial diameter were calculated for each condition. Each individual experiment was performed with sibling larvae from a single batch. Six independent batches were pooled for statistical analysis.

Quantitative real-time PCR (qPCR) of immune genes

Total RNA was extracted from 10 dpf WT and ABCB1a E13-22 crispant larvae at 0, 6, 12, 24 and 48 hpe to *V. diazotrophicus*. For

this, 20–60 larvae were collected per time point directly into lysis buffer for RNA purification and column-based DNase treatment with RNeasy Micro columns (Qiagen), as per the manufacturer's protocol. Two other independent batches of 20-30 larvae were extracted with Trizol (Invitrogen) followed by RNAeasy Micro column clean up. All RNA samples were eluted in 15 µl nucleasefree water. First-strand cDNA was synthesized from 50 ng of each RNA sample by using anchored 1.5 µmol l⁻¹ oligo-dT primers (Integrated DNA Technologies, Coralville, IA, USA), 0.5 mmol l⁻¹ dNTPs (Fermentas, Glen Burnie, MD, USA), 200 U M-MLV Reverse Transcriptase (Promega, Madison, WI, USA) and 25 U RNasin (Promega) at final volume of 25 µl. All cDNA samples were diluted 1:5 with nuclease-free water and used for qPCR. Measurements were made on duplicate samples using an AriaMx Real Time PCR system (Agilent Technologies) with EVA QPCR SuperMix kit reactions (Biochain), as previously described (Shipp and Hamdoun, 2012). Gene expression levels were normalized to 18S rRNA measurements. Relative gene expression data are reported as fold-differences between uninfected larvae (0 hpe) and Vibrio-exposed larvae at 6, 12, 24 and 48 hpe time points, calculated from six internal replicates from three pooled independent batches. Sp-IL17-1, Sp-IL17-4 (Buckley et al., 2017) and Sp-18S primers are listed in Table S1.

Statistical analysis

The Shapiro–Wilks test was used to determine whether data were normally distributed (Razali and Wah, 2011). CRISPR cutting efficiency data, as determined by ICE, were normally distributed and statistical significance was determined by running an unpaired, two-tailed Student's *t*-test. Transporter efflux activity assay data were not normally distributed; therefore, statistical significance was determined by running a two-tailed Mann–Whitney U-test. Gut and pigment cell data from microbial infection assays were not normally distributed and thus were analyzed by one-way ANOVA, and differences between groups were compared by Kruskal–Wallis and *post hoc* Dunn's tests with a significance threshold of $P \le 0.05$. For qPCR data, Student t-tests or Mann–Whitney tests were performed to determine significance between conditions at each time point ($P \le 0.05$). Error bars in all figures represent the standard error of the mean.

RESULTS

Sea urchin ABCB1a expression is enriched in gut tissues of larvae

To define the spatial patterns of *Sp-ABCB1a* expression, and thus its potential locations of action within the embryo, we first localized its expression. Consistent with prior analyses (Shipp and Hamdoun, 2012; Tu et al., 2014), we found that *Sp-ABCB1a* transcripts were present in the unfertilized egg and remained ubiquitous throughout the blastula stages (Fig. 1A–C). By the gastrula stage, the gut tube is morphologically uniform but fated to form three future digestive compartments (Annunziata et al., 2014): the foregut (esophagus), the midgut (stomach; which is the primary site for digestion and absorption in sea urchin larvae; Burke, 1981; Annunziata et al., 2019), and the hindgut (intestine). Near the end of gastrulation, *Sp-ABCB1a* remains expressed in the ectoderm, but becomes enriched in the hindgut and midgut (Fig. 1D). By larval stages, *Sp-ABCB1a* expression is mostly enriched in the stomach and intestine (Fig. 1E,F).

Efficiency of CRISPR/Cas9 mutagenesis in crispants verified using T7E1 and ICE

We next targeted *Sp-ABCB1a* with CRISPR/Cas9. A challenge to using this approach in the F₀ generation is the potential for

confounding effects, such as inefficient cutting or mosaicism (Burger et al., 2016; Hoshijima et al., 2019). Furthermore, the knockout of protective genes such as *ABCB1a* may not produce conspicuous morphological phenotypes until the animals are challenged (Schinkel et al., 1994), making it essential to streamline the effectiveness of the CRISPR-mediated perturbation prior to downstream challenges.

Therefore, to most efficiently target Sp-ABCB1a, we utilized synthetic, chemically modified sgRNAs which have been shown to be more stable than in vitro transcribed sgRNAs (Hendel et al., 2015). We used several approaches to estimate the Cas9-mediated cutting efficiency of different sgRNAs. The first, the T7E1 assay, is a biochemical assay that employs an endonuclease that recognizes and cleaves mismatches in DNA heteroduplexes (Mashal et al., 1995). While this is a longstanding method for detecting larger indels following CRISPR/Cas9 mutagenesis (Hwang et al., 2013: Ota et al., 2014; Thomas et al., 2014), it is not quantitative, and can produce false positives. Thus, we also used a Sanger sequencingbased CRISPR analysis computational tool, ICE, to fully characterize the T7E1 positive sgRNAs. ICE estimates the editing efficiency by comparing sequence degeneracy in crispant sequence reads near the sgRNA target site relative to the WT sequence reads (Hsiau et al., 2019 preprint; Ying and Beronja, 2020).

Determining the efficiency of synthetic sgRNA E1-157 to nodal

We first grounded our approach in the comparison of synthetic sgRNAs with a previously described sgRNA targeting the *S. purpuratus nodal* gene (sgRNA E1-157; Fig. S1A; Table 1). This sgRNA was shown to cause a radialized embryo phenotype, indicative of *Sp-nodal* disruption, in 76% of injected embryos (Lin and Su, 2016). Of 418 Nodal crispant embryos we generated using the synthetic version of sgRNA E1-157, roughly 81% were clearly radialized (Fig. S1B), slightly higher than the level observed by *in vitro* transcribed guides in Lin and Su, 2016.

Next, we analyzed these crispants by T7E1 and ICE assays to establish the baseline for efficient perturbation. T7E1 gels of 'mixed' embryos (i.e. containing both embryos showing the radialized phenotype and those that looked normal) clearly revealed digested products (Fig. S1C) and depletion of control bands, indicative of effective CRISPR-induced mutagenesis. When measured by ICE, 68.7±10.1% of reads from these 'mixed' batches of embryos contained indels (Fig. S1D). When only radialized embryos were collected and analyzed by ICE, the corresponding indel percentage increased to 90.3±3.3% (Fig. S1D).

Efficiency of sgRNAs targeting ABCB1a and ABCB1b

Using our synthetic *nodal* sgRNA (E1-157) results as a baseline, we next sought to determine the efficiency of synthetic sgRNAs designed to target *Sp-ABCB1a*. The *Sp-ABCB1a* gene model spans 50.5 kb (Scaffold 19, genome v5) that contains 27–29 exons (Fig. 2A). We also targeted *Sp-ABCB1b*, which encodes a protein that does not efflux the fluorescent small molecules transported by Sp-ABCB1a (Gökirmak et al., 2012), and thus serves as a suitable negative control. *Sp-ABCB1b* is approximately 63 kb (Scaffold 16, genome v5) and contains 24–25 exons (Fig. 2B).

In silico prediction tools were used to prioritize the potential target sites that should maximize efficient, on-target editing with Cas9. This yielded eight gRNAs (Table 1) that targeted either the early N-terminal domain or the first nucleotide (i.e. ATP) binding domain (NBD). T7E1 assays indicated that out of these eight guides, two sgRNAs targeting the first NBD of *Sp-ABCB1a* (B1a E12-82 and B1a E13-22) and one sgRNA targeting an N-terminal region of

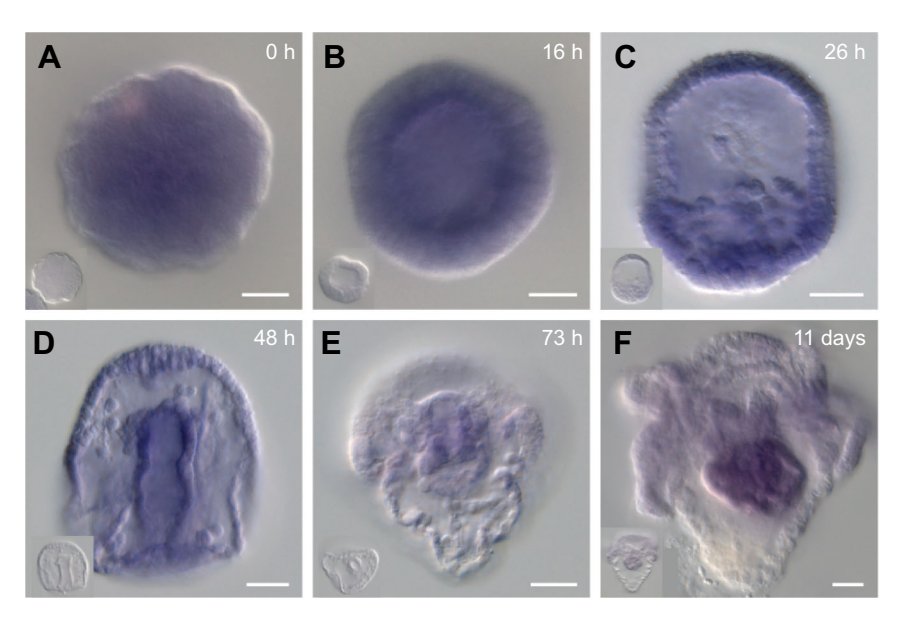


Fig. 1. Sp-ABCB1a is enriched in the gut of Strongylocentrotus purpuratus sea urchin larvae. Sp-ABCB1a transporter transcripts were visualized by whole-mount in situ hybridization. Early in development, global staining indicates ubiquitous constitutive expression from egg (A) to early blastula (B), mesenchyme blastula (C) and gastrula stages (D). By gastrula stages, ABCB1 also becomes enriched in the entire gut tube. At larval (E) and late feeding larval stages (F), ABCB1 remains enriched in the midgut (stomach). Control sense probe images are shown as insets within each panel. Scale bars: 20 μ m.

Sp-ABCB1b (B1b E4-33) induced strong Cas9-mediated endonuclease activity (Fig. 2C). The remaining sgRNAs exhibited minimal or no cutting activity (Fig. S2). ICE analysis of the three T7E1-positive sgRNAs demonstrated an average indel percentage of 72.7±14.7% for B1a E13-22, 21.5±8.8% for B1a E12-82 and 60.3±3.3% for B1b E4-33 sgRNAs (Fig. 2D). Example indels for each gene are shown in Fig. 2E. Based on these results, we prioritized B1a E13-22 and B1b E4-33 crispants for subsequent work.

ABCB1a crispants have decreased efflux activity

As expected from previous studies in *ABCB1* knockout mice (Schinkel et al., 1994), both ABCB1a E13-22 and ABCB1b E4-33 crispants did not have outward morphological defects (Fig. S3). To determine whether these crispants exhibited changes in transporter activity, 72 hpf embryos were incubated with either Bver or CAM, both known fluorescent substrates of Sp-ABCB1a (Gökirmak et al., 2012), and embryos were assayed for substrate accumulation (Fig. 3A–D). The 72 hpf time point was chosen to allow for complete depletion of maternal mRNA and/or protein (Shipp and Hamdoun, 2012).

ABCB1a crispants exhibited increased accumulation of both CAM and Bver as compared with control (WT) embryos (Fig. 3A), while there were no changes in accumulation of substrates in ABCB1b crispants (Fig. 3B). ABCB1a crispants exhibited 3.0 ± 0.3 -fold and 1.9 ± 0.1 -fold increases in accumulation of CAM and Bver, respectively, which was significantly more than ABCB1b crispants (Fig. 3C,E; P<0.001). ABCB1b crispants did not exhibit significant increases in the accumulation of CAM and Bver, relative to control embryos (P>0.050).

As Sp-ABCB1a is not the only transporter known to efflux Bver and CAM from sea urchin embryos, we sought to determine the relative contribution of ABCB1a to the efflux of these substrates. We therefore compared the level of substrate accumulation in ABCB1a crispants with that of WT embryos incubated with PSC833 (Fig. 3D–F), a broad inhibitor of all P-gp transporters (Smith et al., 2000; Gökirmak et al., 2014; Morita and Terada, 2014). Crispants exhibited $23.9\pm2.8\%$ and $39.3\pm4.6\%$ accumulation of Bver and CAM, respectively, relative to PSC833-inhibited controls (Fig. 3F; P<0.001). There were no significant differences between WT and ABCB1a crispants when both were exposed to PSC833 (Fig. S4).

However, PSC8333-inhibited crispants accumulated significantly more CAM (P<0.010) and Bver (P<0.001) than non-inhibited crispants (Fig. S4). This suggests that there exist related transporters that are non-specifically inhibited by PSC833, but are not disrupted by ABCB1a sgRNAs.

MASO-mediated knockdown of *Sp-ABCB1a* recapitulates B1a E13-22 crispant substrate accumulation phenotypes

To validate the efflux phenotypes generated by our CRISPR experiments, we used an *Sp-ABCB1a*-specific ATG-blocking MASO to knockdown expression at the translation level. Embryos were injected with either the *ABCB1a* MASO or a control MASO (Table S1) and incubated with Bver and CAM at the gastrula stage (Fig. 4A,B). We focused on this developmental stage to balance between the effectiveness of MASOs, which can be depleted in later development, and turnover of maternal ABCB1a protein, which occurs at the hatching blastula stage (Shipp and Hamdoun, 2012). ABCB1a morphants exhibited 4.3±0.2- and 2.5±0.2-fold increases in CAM and Bver accumulation (Fig. 4C; *P*<0.001) relative to controls, and consistent with the increased accumulation of both ABCB1 substrates in crispants.

Sp-ABCB1a crispants exhibit increased gut inflammation upon exposure to pathogenic *Vibrio* bacteria

Having established a reliable protocol for the generation of ABCB1a crispants, we next sought to determine how Sp-ABCB1a may function to protect against microbes. Given that *Sp-ABCB1a* is expressed strongly in feeding larval guts (Fig. 1F) and responds transcriptionally to bacterial infection, we hypothesized that Sp-ABCB1a could play a prominent role in protecting larvae from the opportunistic pathogen *V. diazotrophicus*. To examine this potential role, we measured two cellular parameters of the immune response following bacterial exposure (Ho et al., 2016): gut epithelial width and pigment (immune) cell migration towards the gut at 24 and 48 hpe (Fig. 5A).

At 10 dpf, and prior to pathogenic bacteria exposure (0 hpe), crispant larvae exhibited a slightly larger gut epithelial width compared with control (WT) animals (Figs 5A and 6A; P<0.0013), suggesting a possible role for ABCB1 in the efflux of algal metabolites, or for maintaining gut barrier integrity. However, there was no difference in pigment cell location between WT and crispant

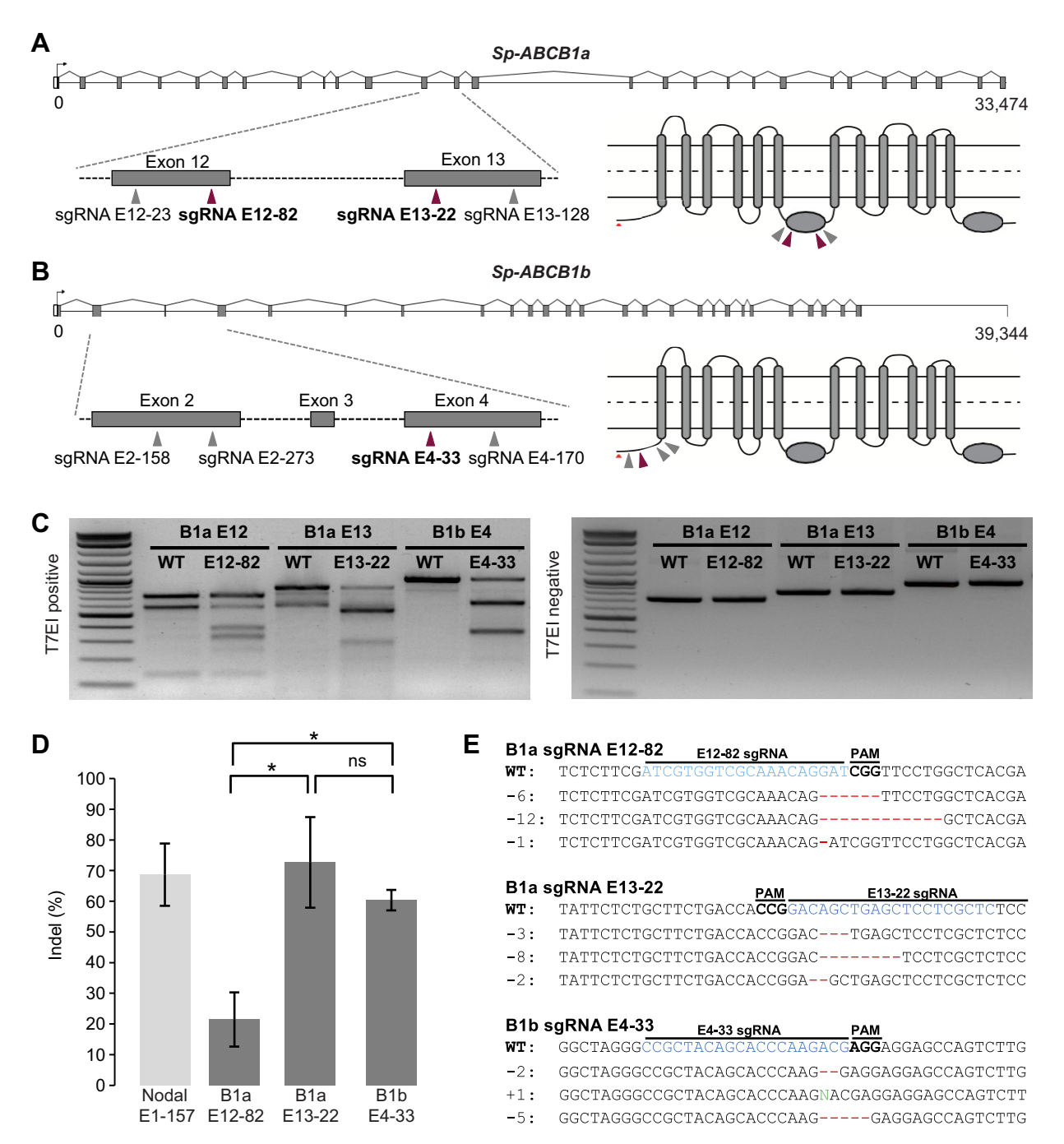


Fig. 2. CRISPR editing efficiency of sgRNAs targeting Sp-ABCB1a and Sp-ABCB1b. (A,B) Gene structure and protein topology models of *S. purpuratus ABCB1a* (A) and *ABCB1b* (B). Each ABC transporter is composed of two transmembrane domains (TMD) consisting of six transmembrane helices each (gray), and two intracellular nucleotide binding domains (NBDs; gray ovals) that mediate active transport. All sgRNAs target the early N-terminal region or first NBD. Red arrowheads indicate target sites of the most efficient sgRNAs as determined by T7E1 assays. (C) T7E1 assays of select sgRNAs. Products were run on a 2% agarose gel (WT, wild-type larvae). Left panel shows products incubated with T7E1. Right panel shows denatured and reannealed heteroduplexes without the addition of T7E1. (D) Inference of CRISPR Edits (ICE) analysis of sgRNA cutting efficiency. Predicted indel percentages are shown. *P<0.05. n=3-6 biological replicates per sgRNA. (E) Example indels sequenced from crispants. PAM, protospacer adjacent motif.

larvae at 10 dpf (Fig. 6B,D; *P*=0.1899), indicating relatively low levels of immune activation.

Next, food (*R. lens*) was removed and larvae were exposed to *V. diazotrophicus* for 48 h (Fig. 5A). Both crispants and controls exhibited the stereotypical immune response to *Vibrio* infection, in which the midgut epithelium thickens and pigment cells are recruited to the inflamed gut (Fig. 5B–D). However, ABCB1a crispants exhibited significantly larger midgut epithelial widths

(Fig. 6A,C; P<0.0001) and increased numbers of migratory and gutassociated pigment cells (Fig. 6B,D; P<0.0001) compared with controls, at both 24 and 48 hpe. ABCB1a crispants cultured in seawater with neither *Vibrio* nor *R. lens* showed no significant increases in pigment cell migration relative to controls over the same time period (Fig. 6D; P=0.2433). Interestingly, the width of gut epithelia in these animals also returned to normal in the absence of bacteria (Figs 5E and 6C; P>0.9999), suggesting that the initial

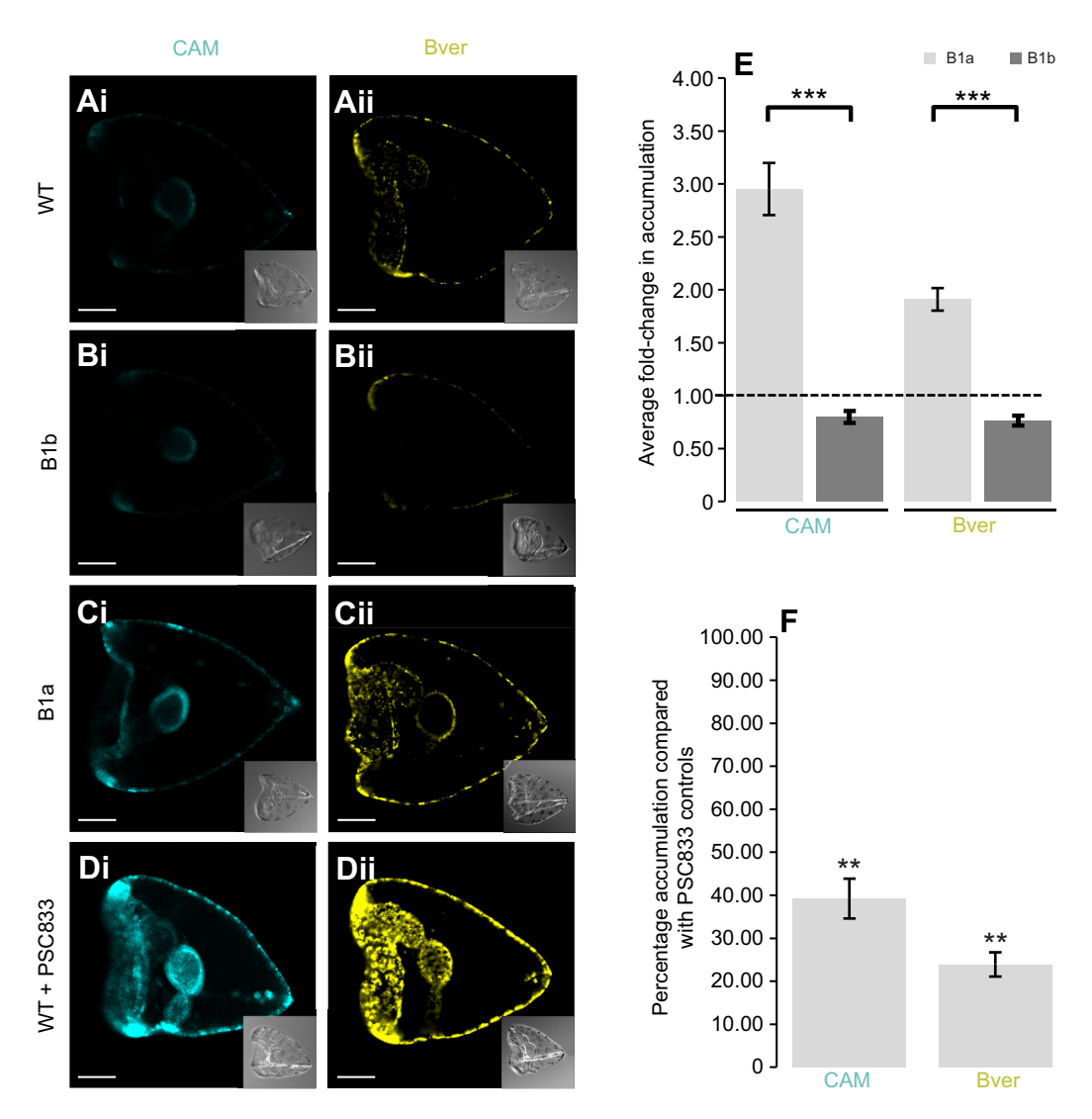


Fig. 3. Reduction of Sp-ABCB1a transporter activity in crispants. (A–D). Confocal micrographs showing accumulation of the ABCB1 substrates calcein-AM (CAM; i) and Bodipy-Verapamil (Bver; ii) at concentrations of 250 and 50 nmol I⁻¹, respectively, by WT (A), B1b E4-33 crispants (B), B1a E13-22 crispants (C) and PSC833-inhibited WT controls (D) at early larval stage (72 hours post-fertilization, hpf). Insets show differential interference contrast (DIC) images of the respective fluorescent embryos. (E) Bar graphs representing the average fold-change in CAM and Bver accumulation in B1a E13-22 compared with B1b E4-33 (control) embryos. *n*=30–51 embryos from 3–5 biological replicates. *****P*<0.001. (F) Bar graph representing the contribution of Sp-ABCB1a to the efflux of Bver and CAM. The *y*-axis shows the percentage accumulation of each substrate in B1a E13-22 crispants compared with PSC833-inhibited controls. *n*=44–51 embryos in 4–5 biological replicates. ****P*<0.01. Scale bars: 50 μm.

differences observed prior to *Vibrio* exposure were a transient response to the *R. lens* cultures used to feed the larvae.

Sp-ABCB1a crispants exhibit a higher level of Sp-IL-17 expression compared with controls

Given the observed responses of crispant larvae to *Vibrio* infection, we tested whether they also experienced amplified immune gene expression (Fig. 6E; Fig. S5). We focused on conserved IL-17 cytokines known to be activated in the gut epithelium after *Vibrio* exposure (Buckley et al., 2017). ABCB1a crispants infected *Vibrio* exhibited higher levels of both *Sp-IL-17-1* and *Sp-IL-17-4* cytokine activation compared with *Vibrio*-infected control larvae (Fig. 6E; Fig. S5). At 10 dpf and prior to the *Vibrio* exposure (0 hpe), there was no significant difference in the relative expression of *Sp-IL-17-1* (*P*=0.2073) or *Sp-IL-17-4* (*P*=0.8182) between crispants and control larvae (Fig. S5A,F). While *Sp-IL-17-1*

expression peaked and attenuated quickly in the infected control larvae (Fig. S5B–E), crispant larvae exposed to *Vibrio* had significantly sustained Sp-IL-17-1 activation at 24 hpe (Fig. S5D; P=0.0262) and 48 hpe (Fig. 6E; Fig. S5E; P=0.0500). By 48 hpe, infected control larvae exhibited a 1.7 ± 0.3 -fold increase in Sp-IL-17-1 expression compared with un-infected control larvae, whereas expression in *Vibrio*-infected ABCB1 crispant larvae remained higher, with a 8.9 ± 2.3 -fold change relative to un-infected crispants (Fig. 6E; Fig. S5E).

Crispant larvae also had a 21.3 ± 8.9 -fold increase in Sp-IL-17-4 expression, compared with a 2.6 ± 1.4 -fold increase in control larvae at 48 hpe (Fig. S5J; P=0.0411), consistent with previous reports that Sp-IL-17-4 is downstream of Sp-IL-17-1 signaling (Buckley et al., 2017). In sum, these results indicate significantly enhanced activation and later dysregulation of gut epithelial cytokine signaling in the absence of Sp-ABCB1a.

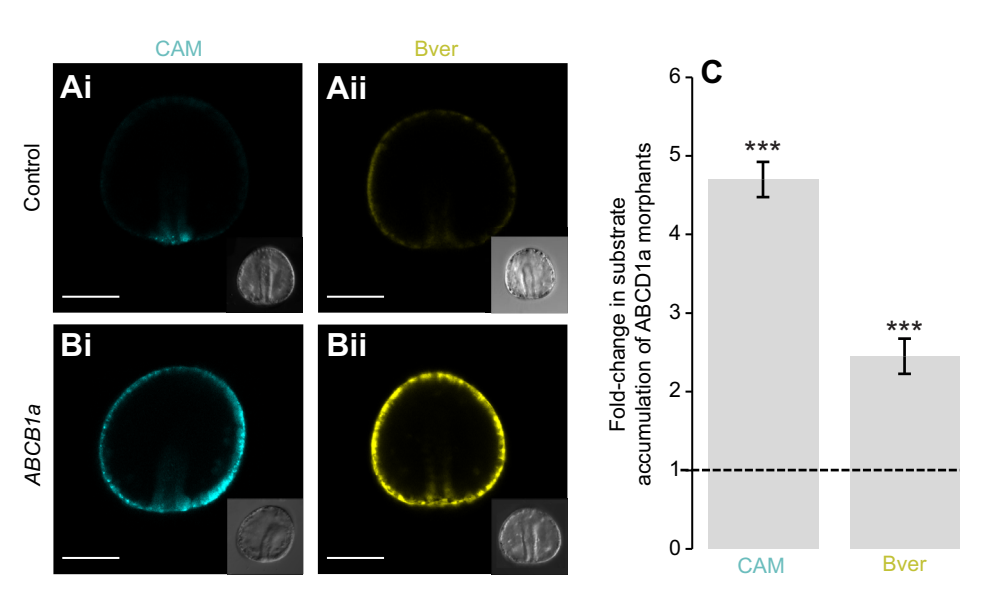


Fig. 4. Transporter efflux activity of *Sp-ABCB1a* morphants. (A,B) Confocal micrographs showing accumulation of the ABCB1 substrates CAM (i) and Bver (ii) in embryos injected with control morpholino antisense oligonucleotide (MASO) or *ABCB1a* MASO at the gastrula stage (48 hpf). Insets show DIC images of the respective fluorescent embryos. (C) Bar graph representing the average fold-change in accumulation of CAM and Bver in B1a morphants compared with control embryos. *n*=20–27 embryos in 2–3 biological replicates. *****P*<0.001. Scale bars: 50 μm. *ABCB1a* MASO or a control MASO.

DISCUSSION

CRISPR/Cas9 genome editing is quickly becoming a reliable mutagenesis technique in marine animals including sea anemones, diatoms and lampreys (Square et al., 2015; Nymark et al., 2017; Nakanishi and Martindale, 2018). A contribution of this study is to outline how CRISPR/Cas9-mediated gene editing can be optimized towards understanding the function of transporter genes in the sea urchin larva, which may not have obvious morphological phenotypes prior to xenobiotic challenge. In this case, we used a

modified approach to dissect the function of Sp-ABCB1a and revealed a potential endogenous role in host-microbe interactions.

Considerations for CRISPR/Cas9 mutagenesis of ABC transporters and analysis of phenotypes in the F₀ generation

An attractive feature of the sea urchin as a model organism is the ability to rapidly generate large numbers of embryos, which can easily be genetically modified to produce F_0 crispants. However, CRISPR/Cas9-mediated editing has highly variable efficiency in

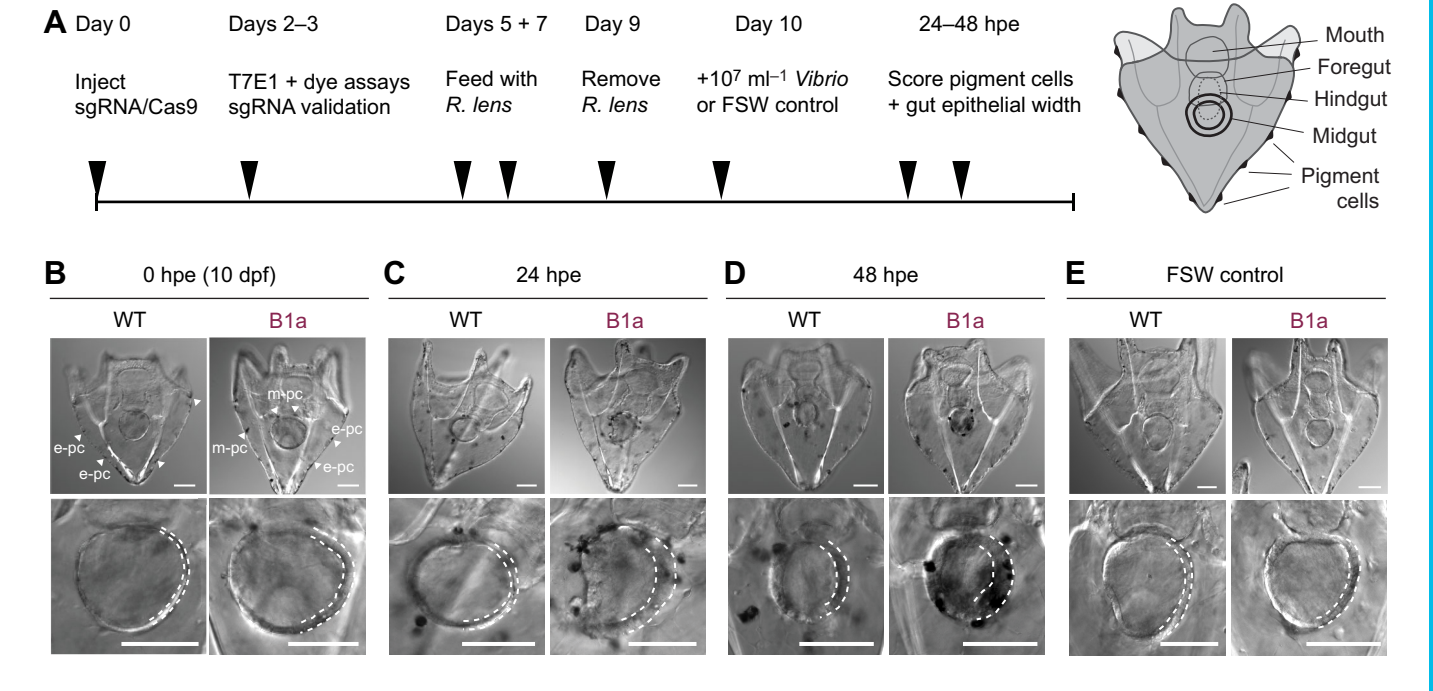


Fig. 5. CRISPR-mediated knockout of *Sp-ABCB1a* increases inflammatory responses in larvae exposed to *Vibrio* bacteria. (A) Experimental design. ABCB1a E13-22 crispants and control (WT) larvae were grown and fed (with *Rhodomonas lens*) up to 9 days post-fertilization (dpf). At 10 dpf, larvae were exposed to *Vibrio diazotrophicus* (10⁷ ml⁻¹ filtered sea water, FSW), or FSW alone as a control. At 24 and 48 h post-exposure (hpe), larvae were imaged and scored for midgut (stomach) epithelial morphology and pigment cell migration to the gut. (B–E) ABCB1a E13-22 crispants exhibit enhanced gut epithelial inflammation. Representative images of WT control and B1a crispant larvae are shown at 0 hpe (B), 24 hpe (C) and 48 hpe (D) to *Vibrio*, with a 48 h FSW control (E). White arrowheads in B highlight examples of epithelium-localized pigment cells (e-pc) and migratory pigment cells (m-pc). The bottom panels show magnified focal planes focused on the midgut epithelia (partially outlined by the white dashed line). Crispants had a larger midgut epithelia width and often exhibited a rougher, more vesicle-filled epithelium compared with control larvae. Scale bars: 50 μm.

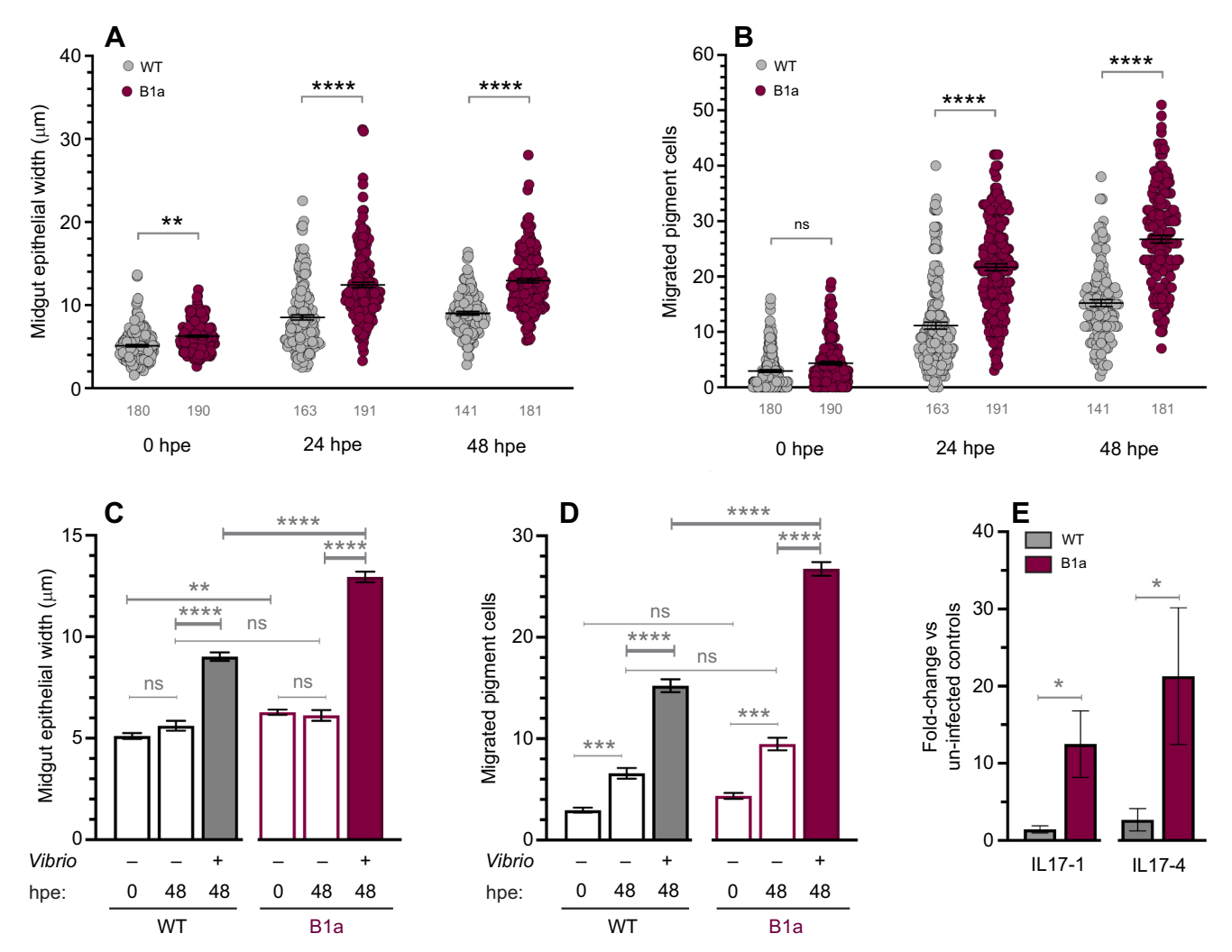


Fig. 6. Increased gut inflammation, cell migration and *IL-17* cytokine expression in ABCB1a E13-22 crispant larvae after *Vibrio* exposure. (A,B) Midgut epithelial width (A) and migrated pigment cell numbers (B) pre- and post-infection. The number of larvae in each condition is shown below the *x*-axis in gray. Differences between groups were compared by one-way ANOVA (Kruskal–Wallis and *post hoc* Dunn's tests with a threshold of *P*≤0.05). ***P*=0.0013, ******P*<0.0001. *n*=141–191 larvae per time point and condition, pooled from six independent batches. (C,D) Midgut epithelial width (C) and migrated pigment cell numbers (D) in control and B1a crispant larvae exposed (+) or not (FSW alone; −) to *Vibrio*. Differences between groups were compared by one-way ANOVA as in A and B. *n*=62–191 larvae per time point and condition, pooled from six independent batches. (C) Prior to exposure, crispant larvae exhibited larger gut epithelial width than controls. However, by 48 hpe, gut epithelia were no longer different between WT and crispant larvae exposed to FSW alone (*P*>0.9999), whereas *Vibrio*-exposed crispants had significantly larger epithelial width than *Vibrio*-exposed control larvae (***P*=0.0013; *****P*<0.0001). (D) Crispant larvae exposed to *Vibrio* also exhibited significant increases in pigment cell migration at 48 hpe compared with matched FSW controls (****P*=0.0001; ****P*<0.0001). (E) *IL-17* cytokine transcript prevalence was measured using qPCR. Expression values were normalized to 18S rRNA and are reported as the mean fold-difference of *Vibrio*-exposed larvae (48 hpe) to un-infected larvae. Unpaired *t*-tests with Welch's correction (*IL-17-1*; **P*=0.0500) or Mann–Whitney tests (*IL-17-4*; **P*=0.0411). *n*=6 internal replicates from three biological replicates. Crispant *IL-17* expression also trended earlier and higher than WT control expression at 6–24 hpe (Fig. S5).

the F₀ generation, dependent on numerous factors including: the choice of physical delivery method, molecular delivery of CRISPR components, sgRNA length and sequence, cell type and organism (Zhang et al., 2016; Lino et al., 2018). In sea urchins, this technique has only been used in a handful of studies to date (Lin and Su, 2016; Shevidi et al., 2017; Liu et al., 2019; Wessel et al., 2020; Yaguchi et al., 2020), all of which have targeted genes in which a mutation confers an easily visualized, and previously established, phenotype. In order to assess more cryptic phenotypes of *Sp-ABCB1a*, we screened for synthetic sgRNAs with relatively high efficiency in producing indels. *Sp-ABCB1a* sgRNAs with over 70% cutting efficiency proved effective at reducing transport function, generating up to a 3-fold increase in ABCB1a substrate accumulation (Fig. 2).

Compared with other mutagenesis studies in the sea urchin (Lin and Su, 2016), our gene editing efficiency appeared slightly improved by the use of chemically modified synthetic sgRNAs (81% versus standard 76% visible *Sp-nodal* phenotype; Fig. S1), which may have greater stability than *in vitro* transcribed guides (Hendel et al., 2015). Previous studies indicate that sgRNAs enriched with guanine also exhibit more stability (Huppert et al., 2008; Moreno-Mateos et al., 2015). Additionally, a cytosine at the –3 position (3' relative to the protospacer adjacent motif, PAM) and an adenine or guanine at the –1 position are often correlated with higher sgRNA activity (Doench et al., 2014; Ren et al., 2014; Wong et al., 2015; Xu et al., 2015). However, the three most efficient sgRNAs used in our study (*nodal* E1-157, *ABCB1a* E13-22, *ABCB1b* E4-33) conferred relatively similar efficiencies despite containing varying amounts of guanine,

and did not follow the -3/-1 trend (Table 1, Fig. 2D). These results could simply be an artifact of the smaller number of sgRNAs tested (8), or suggest that parameters for predicting sgRNA stability and efficiency can vary between model systems.

A conserved role for ABCB1 in host-microbe interactions in gut epithelia

This study demonstrated that *Sp-ABCB1a* is enriched in the gut tissues of sea urchin embryos and larvae (Fig. 1) and that, in the absence of Sp-ABCB1a, the larval gut experienced a transient increase in baseline epithelial inflammation after feeding on *R. lens* (Figs 5 and 6). Further exposure to the opportunistic pathogen *V. diazotrophicus* in crispants led to significantly increased gut pathology, stronger recruitment of pigment cells to the inflamed gut, and an elevated pro-inflammatory *Sp-IL-17* cytokine response, as compared with infected control larvae (Fig. 6; Fig. S5). These observations strongly suggest a role for ABCB1a in managing gut microbial products.

It has been hypothesized that in mammals, the expression of ABC transporters is specifically necessary to reduce epithelial exposure to harmful products of enteric bacteria (Mercado-Lubo, 2010; Cario, 2017). Intriguingly, one of the 'unanticipated' phenotypes in the first ABCB1 knockout mouse was the observation that mice lacking this protein in gut epithelial cells spontaneously develop inflammatory bowel diseases such as colitis (Panwala et al., 1998). $Mdr1^{-/-}$ mice exhibit a pronounced thickening of the mucosa and immune cell infiltration in the gut. Importantly, the pathology is entirely dependent on the presence of the commensal microbes. In turn, challenges with pathogenic bacteria, such as *Helicobacter*, *Listeria* and *Salmonella*, accelerate the occurrence and severity of gut inflammation (Maggio-Price et al., 2002; Neudeck et al., 2004; Siccardi et al., 2008).

Our results in the sea urchin larva mirror those observed in knockout mammals and may extend to downstream immune signaling (Figs 5 and 6; Fig. S5). In both mice and sea urchins, *IL-17* genes are activated by bacteria in the gut mucosa, and an autocrine IL-17 cascade controls downstream signaling and effector genes that recruit immune cells to the gut and help repair tissue damage from inflammation (Ramirez-Carrozzi et al., 2011; Song et al., 2011; Buckley et al., 2017). However, an inability to properly control IL-17 cytokine responses can lead to even more tissue damage. *IL-17C* becomes aberrantly induced in dextran sulfate sodium (DSS)-induced colitis models (Ramirez-Carrozzi et al., 2011), but to our knowledge, *IL-17* responses have yet to be described in *mdr1*^{-/-} mice. Our results are the first to suggest that in the absence of ABCB1, IL-17 signaling can be activated at greater levels and for longer periods of time following bacterial infection (Fig. 6E; Fig. S5).

Inflammatory phenotypes in Sp-ABCB1a crispants before and after bacterial exposure

We observed a transient gut epithelial phenotype in Sp-ABCB1a crispant larvae prior to *Vibrio* infection (Figs 5E and 6A). This could be interpreted as a potential direct function of Sp-ABCB1a in maintaining barrier integrity *de novo*, which has been demonstrated in the blood–testes barrier of mammals (Su et al., 2009; Su et al., 2011). However, larval guts appear normal in earlier development stages (Fig. S3), and the initial gut inflammatory phenotype was not maintained when larvae were cultured for a further 48 h in the absence of algae or *Vibrio* (Fig. 6C). Therefore, we suspect that the inflammation in crispants results mostly from the bacterial infection, rather than from a direct role of Sp-ABCB1a in maintaining barrier integrity.

Lab cultures of the larval diet species R. lens are typically not axenic; thus, crispant animals may initially be responding to both

xenobiotic algal compounds (Eufemia et al., 2000) and products from algae-associated bacteria (Mercado-Lubo, 2010; Dorrestein et al., 2014; Ganal-Vonarburg et al., 2020). Feeding is the primary driver of microbial colonization in sea urchin larvae in the wild and in the lab (Carrier and Reitzel, 2018; Schuh et al., 2020). Anecdotally, we have observed that crispants will survive to adulthood and reproduce under normal culturing conditions (unpublished results). This suggests that the function of ABCB1 is most critical for defense against pathogenic strains of bacteria, rather than against commensals.

Here, we hypothesize that Sp-ABCB1a transporter activity most likely aids in the elimination of Vibrio-derived compounds. A buildup of these factors in crispants may subsequently drive the trio of stronger inflammatory responses we have observed. Potential Sp-ABCB1a substrates could include a variety of molecules generated by bacteria. By 24 hpe. V. diazotrophicus will translocate out of the gut epithelium into the body cavity (Ho et al., 2016), indicating the utilization of virulence factors. These may include known zonula occludens toxins (Castillo et al., 2018a,b), and small diffusible molecules required for quorum sensing, niche establishment and virulence (Yang et al., 2011; Girard, 2019). Additional pathogenicity factors could be secreted extracellular proteases and toxins (Farto et al., 2006; Nottage and Birkbeck, 1986; Schuh et al., 2020) that are generated through Type-II secretion systems prominent in Vibrio species (Cianciotto and White, 2017). Future studies will identify and validate Sp-ABCB1a substrates derived from V. diazotrophicus and other opportunistic bacteria in sea urchin larvae.

Potential ecological implications of ABCB1-mediated hostmicrobe interactions

Cellular mechanisms of protection from xenobiotics often evolve in concert with their respective environment (Bard, 2000; Hamdoun and Epel, 2007; Li et al., 2007; Calla et al., 2017). The xenobiotic metabolism genes of insects have diversified and acquired novel functions in gut tissues, depending on the plant or microbe-derived substrates that are encountered in their diets (Berenbaum, 2002). In yeast, paralogs of ABC transporters rapidly evolve substrate specificity to different factors in the environment (Srikant et al., 2020). In Atlantic killifish, expanded and highly polymorphic aryl hydrocarbon receptor and cytochrome P450 gene families have enabled subpopulations of fish to adapt to highly polluted environments (Whitehead et al., 2012, 2017).

In the sea urchin, ABC transporter and related detoxification genes are likewise expanded, compared with vertebrate homologs (Goldstone et al., 2006; Hamdoun and Epel, 2007). The *Sp-ABCB1a* gene is also polymorphic (unpublished observations). This polymorphism could have implications for the ability of different subpopulations of larvae to handle local microbes, as these animals occupy a very wide geographic range, from the coasts of southern Alaska, USA, to Baja California, Mexico (Thompson et al., 2017; Carrier and Reitzel, 2018). Given that global warming and increased pollution are predicted to cause large-scale modulations of microbial communities in the world's oceans (Hellweger et al., 2014; Walworth et al., 2020), ABC transporters could make subpopulations of *S. purpuratus* more or less vulnerable to environmental microbial changes or related dysbiosis in the gut.

Conclusions

The question of what small molecule transporters 'really do' (Nigam, 2015) is one that has eluded the field for decades. While ABC transporters certainly play important roles in drug disposition (International Transporter Consortium et al., 2010), they did not

evolve to make life difficult for pharmacologists. CRISPR/Cas9 genome editing has provided a possible solution to this problem, making it relatively easy to modify genomes and perturb protein function (Jinek et al., 2012). Our localization data and improved CRISPR/Cas9 methodology in the sea urchin larva have revealed a potentially conserved role for ABCB1 in microbial defense at the gut mucosa. *Strongylocentrotus purpuratus* is becoming a robust model for understanding fundamental aspects of gut homeostasis and immunity at the cellular, molecular and biochemical level (Buckley and Rast, 2019; Carrier and Reitzel, 2020; Stumpp et al., 2020). Our work establishing reproducible echinoderm ABCB1 crispants will allow us to begin dissecting functional mechanisms of ABCB proteins in host—microbial settings, which are relevant for predicting how marine larvae may adapt to future ocean environments.

Acknowledgements

The authors thank Elliot Jackson, Drs Vic Vacquier and Bianca Brahamsha, and two anonymous JEB reviewers for their insightful critique and comments on the manuscript.

Competing interests

The authors declare no competing or financial interests.

Author contributions

Conceptualization: T.F., C.S.S., H.V., H.D.R., A.H.; Methodology: T.F., C.S.S., H.V., A.H.; Software: A.H.; Validation: T.F., C.S.S., H.V.; Formal analysis: T.F., C.S.S., H.V., A.H.; Investigation: T.F., C.S.S., H.V., H.D.R., A.H.; Resources: A.H.; Data curation: T.F., C.S.S., H.V., Writing - original draft: T.F., C.S.S.; Writing - review & editing: T.F., C.S.S., H.V., H.D.R., A.H.; Visualization: T.F., C.S.S., H.V., A.H.; Supervision: A.H.: Project administration: A.H.: Funding acquisition: C.S.S., A.H.

Funding

This work is supported by National Institutes of Health grants ES 027921 and ES 030318; National Science Foundation grant 1840844 to A.H.; and National Institutes of Health grant F32ES029843 to C.S.S. Deposited in PMC for release after 12 months.

Data availability

Supplementary information

Supplementary information available online at https://jeb.biologists.org/lookup/doi/10.1242/jeb.232272.supplemental

References

- Adolph, S. (2004). Cytotoxicity of diatom-derived oxylipins in organisms belonging to different phyla. *J. Exp. Biol.* **207**, 2935-2946. doi:10.1242/jeb.01105
- Agarwal, V., El Gamal, A. A., Yamanaka, K., Poth, D., Kersten, R. D., Schorn, M., Allen, E. E. and Moore, B. S., (2014). Biosynthesis of polybrominated aromatic organic compounds by marine bacteria. *Nat. Chem. Biol.* 10, 640-647. doi:10. 1038/nchembio.1564
- Aller, S. G., Yu, J., Ward, A., Weng, Y., Chittaboina, S., Zhuo, R., Harrell, P. M., Trinh, Y. T., Zhang, Q., Urbatsch, I. L. et al. (2009). Structure of P-Glycoprotein reveals a molecular basis for poly-specific drug binding. Science 323, 1718-1722. doi:10.1126/science.1168750
- Annunziata, R., Perillo, M., Andrikou, C., Cole, A. G., Martinez, P. and Arnone, M. I. (2014). Pattern and process during sea urchin gut morphogenesis: the regulatory landscape. *Genesis* 52, 251-268. doi:10.1002/dvg.22738
- Annunziata, R., Andrikou, C., Perillo, M., Cuomo, C. and Arnone, M. I., (2019).
 Development and evolution of gut structures: from molecules to function. *Cell Tissue Res.* 377, 445-458. doi:10.1007/s00441-019-03093-9
- Bard, S. (2000). Multixenobiotic resistance as a cellular defense mechanism in aquatic organisms. Aquatic Toxicology, 48, 357-389. doi:10.1016/S0166-445X(00)00088-6
- Berenbaum, M. R. (2002). Postgenomic chemical ecology: from genetic code to ecological interactions. J. Chem. Ecol. 28, 873-896. doi:10.1023/A:1015260931034
- Bošnjak, I., Uhlinger, K. R., Heim, W., Smital, T., Franekić-Ćolić, J., Coale, K., Epel, D. and Hamdoun, A. (2009). Multidrug efflux transporters limit accumulation of inorganic, but not organic, mercury in sea urchin embryos. *Environ. Sci. Technol.* 43, 8374-8380. doi:10.1021/es901677r
- Buckley, K. M. and Rast, J. P. (2019). Immune activity at the gut epithelium in the larval sea urchin. *Cell Tissue Res.* **377**, 469-474. doi:10.1007/s00441-019-03095-7

- Buckley, K. M., Ho, E. C. H., Hibino, T., Schrankel, C. S., Schuh, N. W., Wang, G. and Rast, J. P. (2017). IL17 factors are early regulators in the gut epithelium during inflammatory response to Vibrio in the sea urchin larva. *eLife* 6. doi:10. 7554/eLife.23481
- Burger, A., Lindsay, H., Felker, A., Hess, C., Anders, C., Chiavacci, E., Zaugg, J., Weber, L. M., Catena, R., Jinek, M. et al. (2016). Maximizing mutagenesis with solubilized CRISPR-Cas9 ribonucleoprotein complexes. *Development* 143, 2025-2037. doi:10.1242/dev.134809
- Burke, R. D. (1981). Structure of the digestive tract of the pluteus larva of Dendraster excentricus (Echinodermata: Echinoida). Zoomorphology, 98, 209-225. doi:10. 1007/BF00312050
- Calla, B., Noble, K., Johnson, R. M., Walden, K. K. O., Schuler, M. A., Robertson, H. M. and Berenbaum, M. R. (2017). Cytochrome P450 diversification and hostplant utilization patterns in specialist and generalist moths: Birth, death and adaptation. *Mol. Ecol.* 26, 6021-6035. doi:10.1111/mec. 14348
- Calle, F. (2017). Marine microbiome as source of natural products. *Microbial Biotechnol.* 10, 1293-1296. doi:10.1111/1751-7915.12882
- Campos, B., Altenburger, R., Gómez, C., Lacorte, S., Piña, B., Barata, C. and Luckenbach, T. (2014). First evidence for toxic defense based on the multixenobiotic resistance (MXR) mechanism in Daphnia magna. *Aquat. Toxicol.* 148, 139-151. doi:10.1016/j.aquatox.2014.01.001
- Cario, E. (2017). P-glycoprotein multidrug transporter in inflammatory bowel diseases: more questions than answers. World J. Gastroenterol. 23, 1513-1520. doi:10.3748/wjg.v23.i9.1513
- Carrier, T. J. and Reitzel, A. M. (2018). Convergent shifts in host-associated microbial communities across environmentally elicited phenotypes. *Nat. Commun.* **9**, 952. doi:10.1038/s41467-018-03383-w
- Carrier, T. J. and Reitzel, A. M. (2020). Symbiotic life of echinoderm larvae. Front. Ecol. Evol. 7. doi:10.3389/fevo.2019.00509
- Castillo, D., Vandieken, V., B. Engelen, T. Engelhardt, and M. and Middelboe, (2018a). Draft genome sequences of six vibrio diazotrophicus strains isolated from deep subsurface sediments of the baltic sea. *Genome Announcements* 6. doi:10.1128/genomeA.00081-18
- Castillo, D., Kauffman, K., Hussain, F., Kalatzis, P., Rørbo, N., Polz, M. F. and Middelboe, M., (2018b). Widespread distribution of prophage-encoded virulence factors in marine Vibrio communities. Sci. Rep. 8, 9973. doi:10.1038/s41598-018-28326-9
- Cianciotto, N. P. and White, R. C. (2017). Expanding role of Type II secretion in bacterial pathogenesis and beyond. *Infect. Immun.* **85**, e00014-17. doi:10.1128/IAI.00014-17
- Danø, K. (1973). Active outward transport of daunomycin in resistant ehrlich ascites tumor cells. *Biochim. Biophys. Acta* 323, 466-483. doi:10.1016/0005-2736(73)90191-0
- Dean, M. and Annilo, T. (2005). Evolution of the atp-binding cassette (ABC) transporter superfamily in vertebrates. Annu. Rev. Genomics Hum. Genet. 6, 123-142. doi:10.1146/annurev.genom.6.080604.162122
- Doench, J. G., Hartenian, E., Graham, D. B., Tothova, Z., Hegde, M., Smith, I., Sullender, M., Ebert, B. L., Xavier, R. J. and Root, D. E. (2014). Rational design of highly active sgRNAs for CRISPR-Cas9—mediated gene inactivation. *Nat. Biotechnol.* **32**, 1262-1267. doi:10.1038/nbt.3026
- Dorrestein, P. C., Mazmanian, S. K. and Knight, R. (2014). Finding the missing links among metabolites, microbes, and the host. *Immunity* **40**, 824-832. doi:10. 1016/j.immuni.2014.05.015
- Eufemia, N., Girshick, S. and Epel, D. (2000). Algal products as naturally occurring modulators for the multidrug resistance (MDR) transporter. *Mar. Environ. Res.* **50**, 332-333. doi:10.1016/S0141-1136(00)00199-9
- Faria, M., López, M. A., Fernández-Sanjuan, M., Lacorte, S. and Barata, C. (2010). Comparative toxicity of single and combined mixtures of selected pollutants among larval stages of the native freshwater mussels (Unio elongatulus) and the invasive zebra mussel (Dreissena polymorpha). Sci. Total Environ. 408, 2452-2458. doi:10.1016/j.scitotenv.2010.02.047
- Farto, R., Armada, S. P., Montes, M., Perez, M. J. and Nieto, T. P. (2006). Presence of a lethal protease in the extracellular products of Vibrio splendidus-Vibrio lentus related strains. *J. Fish Dis.* 29, 701-707. doi:10.1111/j.1365-2761. 2006.00746.x
- Fischer, S., Klüver, N., Burkhardt-Medicke, K., Pietsch, M., Schmidt, A.-M., Wellner, P., Schirmer, K. and Luckenbach, T. (2013). Abcb4 acts as multixenobiotic transporter and active barrier against chemical uptake in zebrafish (Danio rerio) embryos. BMC Biol. 11, 69. doi:10.1186/1741-7007-11-69
- Ganal-Vonarburg, S. C., Hornef, M. W. and Macpherson, A. J. (2020). Microbial-host molecular exchange and its functional consequences in early mammalian life. Science (New York, N.Y.) 368, 604-607. doi:10.1126/science.aba0478
- Girard, L. (2019). Quorum sensing in Vibrio spp.: the complexity of multiple signalling molecules in marine and aquatic environments. Crit. Rev. Microbiol. 45, 451-471. doi:10.1080/1040841X.2019.1624499
- Gökirmak, T., Campanale, J. P., Shipp, L. E., Moy, G. W., Tao, H. and Hamdoun, A. (2012). Localization and substrate selectivity of sea urchin multidrug (MDR) efflux transporters. *J. Biol. Chem.* **287**, 43876-43883. doi:10.1074/jbc.M112. 424879

- Gökirmak, T., Shipp, L. E., Campanale, J. P., Nicklisch, S. C. T. and Hamdoun, A. (2014). Transport in technicolor: Mapping ATP-binding cassette transporters in sea urchin embryos. *Mol. Reprod. Dev.* 81, 778-793. doi:10.1002/mrd.22357
- Goldstone, J. V., Hamdoun, A., Cole, B. J., Howard-Ashby, M., Nebert, D. W., Scally, M., Dean, M., Epel, D., Hahn, M. E. and Stegeman, J. J. (2006). The chemical defensome: Environmental sensing and response genes in the Strongylocentrotus purpuratus genome. *Dev. Biol.* 300, 366-384. doi:10.1016/j. vdbio.2006.08.066
- Gros, P., Croop, J., Roninson, I., Varshavsky, A. and Housman, D. E. (1986). Isolation and characterization of DNA sequences amplified in multidrug-resistant hamster cells. *Proc. Natl Acad. Sci. USA*, **83**, 337-341. doi:10.1073/pnas.83.2. 337
- Guerinot, M. L., West, P. A., Lee, J. V. and Colwell, R. R. (1982). Vibrio diazotrophicus sp. nov., a marine nitrogen-fixing bacterium. *Int. J. Syst. Bacteriol.* 32, 350-357. doi:10.1099/00207713-32-3-350
- Hamdoun, A. and Epel, D. (2007). Embryo stability and vulnerability in an always changing world. Proc. Natl. Acad. Sci. USA 104, 1745-1750. doi:10.1073/pnas. 0610108104
- Hamdoun, A. M., Cherr, G. N., Roepke, T. A. and Epel, D., (2004). Activation of multidrug efflux transporter activity at fertilization in sea urchin embryos (Strongylocentrotus purpuratus). Dev. Biol. 276, 452-462. doi:10.1016/j.ydbio. 2004.09.013
- Hellweger, F. L., Van Sebille, E. and Fredrick, N. D. (2014). Biogeographic patterns in ocean microbes emerge in a neutral agent-based model. Science 345, 1346-1349. doi:10.1126/science.1254421
- Hendel, A., Bak, R. O., Clark, J. T., Kennedy, A. B., Ryan, D. E., Roy, S., Steinfeld, I., Lunstad, B. D., Kaiser, R. J., Wilkens, A. B. et al. (2015). Chemically modified guide RNAs enhance CRISPR-Cas genome editing in human primary cells. *Nat. Biotechnol.* 33, 985-989. doi:10.1038/nbt.3290
- Ho, E. C. H., Buckley, K. M., Schrankel, C. S., Schuh, N. W., Hibino, T., Solek, C. M., Bae, K., Wang, G. and Rast, J. P., (2016). Perturbation of gut bacteria induces a coordinated cellular immune response in the purple sea urchin larva. *Immunol. Cell Biol.* 94, 861-874. doi:10.1038/icb.2016.51
- Hoshijima, K., Jurynec, M. J., Klatt Shaw, D., Jacobi, A. M., Behlke, M. A. and Grunwald, D. J. (2019). Highly efficient CRISPR-Cas9-based methods for generating deletion mutations and F0 embryos that lack gene function in Zebrafish. *Dev. Cell.* **5**, 645-657. doi:10.1016/j.devcel.2019.10.004
- Hsiau, T., Conant, D., Rossi, N., Maures, T., Waite, K., Yang, J., Joshi, S., Kelso, R., Holden, K., Enzmann, B. L. et al. (2019). Inference of CRISPR edits from sanger trace data. bioRxiv. doi:10.1101/251082
- Huppert, J. L., Bugaut, A., Kumari, S. and Balasubramanian, S., (2008). G-quadruplexes: the beginning and end of UTRs. *Nucleic Acids Res.* 36, 6260-6268. doi:10.1093/nar/qkn511
- Hwang, W. Y., Fu, Y., Reyon, D., Maeder, M. L., Tsai, S. Q., Sander, J. D., Peterson, R. T., Yeh, J.-R. J. and Joung, J. K., (2013). Efficient genome editing in zebrafish using a CRISPR-Cas system. *Nat. Biotechnol.* 31, 227-229. doi:10. 1038/nbt.2501
- International Transporter Consortium, Giacomini, K. M., Huang, S. M., Tweedie, D. J., Benet, L. Z., Brouwer, K. L., Chu, X., Dahlin, A., Evers, R., Fischer, V. et al. (2010). Membrane transporters in drug development. *Nat. Rev. Drug Discov.* 9, 215-236. doi:10.1038/nrd3028
- Jao, L.-E., Wente, S. R. and Chen, W. (2013). Efficient multiplex biallelic zebrafish genome editing using a CRISPR nuclease system. *Proc. Natl Acad. Sci. USA* 110, 13904-13909. doi:10.1073/pnas.1308335110
- Jinek, M., Chylinski, K., Fonfara, I., Hauer, M., Doudna, J. A. and Charpentier, E., (2012). A programmable dual-RNA-guided DNA endonuclease in adaptive bacterial immunity. *Science* 337, 816-821. doi:10.1126/science.1225829
- Juliano, R. L. and Ling, V. (1976). A surface glycoprotein modulating drug permeability in Chinese hamster ovary cell mutants. *Biochimica et Biophysica Acta (BBA) - Biomembranes*, 455, 152-162. doi:10.1016/0005-2736(76)90160-7
- Le, C. A., Harvey, D. S. and Aller, S. G. (2020). Structural definition of polyspecific compensatory ligand recognition by P-glycoprotein. *IUCrJ* 7, 663-672. doi:10. 1107/S2052252520005709
- Li, X., Schuler, M. A. and Berenbaum, M. R. (2007). Molecular mechanisms of metabolic resistance to synthetic and natural xenobiotics. *Annu. Rev. Entomol.* 52, 231-253. doi:10.1146/annurev.ento.51.110104.151104
- Lin, C. Y. and Su, Y. H. (2016). Genome editing in sea urchin embryos by using a CRISPR/Cas9 system. Dev. Biol. 409, 1-9. doi:10.1016/j.ydbio.2015.11.020
- Lino, C. A., Harper, J. C., Carney, J. P. and Timlin, J. A. (2018). Delivering CRISPR: a review of the challenges and approaches. *Drug Deliv.* 25, 1234-1257. doi:10.1080/10717544.2018.1474964
- Liu, D., Awazu, A., Sakuma, T., Yamamoto, T. and Sakamoto, N. (2019). Establishment of knockout adult sea urchins by using a CRISPR Cas9 system. Dev. Growth Differ. 61, 378-388. doi:10.1111/dgd.12624
- Maggio-Price, L., Shows, D., Waggie, K., Burich, A., Zeng, W., Escobar, S., Morrissey, P. and Viney, J. L. (2002). Helicobacter bilis infection accelerates and H. hepaticus infection delays the development of colitis in multiple drug resistance-deficient (mdr1a-/-) mice. *Am. J. Pathol.* **160**, 739-751. doi:10. 1016/S0002-9440(10)64894-8

- Mashal, R. D., Koontz, J. and Sklar, J. (1995). Detection of mutations by cleavage of DNA heteroduplexes with bacteriophage resolvases. *Nat. Genet.* 9, 177-183. doi:10.1038/ng0295-177
- Mcfall-Ngai, M. J. (2002). Unseen forces: the influence of bacteria on animal development. *Dev. Biol.* **242**, 1-14. doi:10.1006/dbio.2001.0522
- Mcfall-Ngai, M., Hadfield, M. G., Bosch, T. C. G., Carey, H. V., Domazet-Lošo, T., Douglas, A. E., Dubilier, N., Eberl, G., Fukami, T., Gilbert, S. F. et al. (2013). Animals in a bacterial world, a new imperative for the life sciences. *Proc. Natl Acad. Sci. USA* 110, 3229-3236. doi:10.1073/pnas.1218525110
- **Mercado-Lubo, R.** (2010). The interaction of gut microbes with host ABC transporters. *Gut Microbes* **1**, 301-306. doi:10.4161/gmic.1.5.12925
- Moreno-Mateos, M. A., Vejnar, C. E., Beaudoin, J.-D., Fernandez, J. P., Mis, E. K., Khokha, M. K. and Giraldez, A. J. (2015). CRISPRscan: designing highly efficient sgRNAs for CRISPR-Cas9 targeting in vivo. *Nat. Methods* 12, 982-988. doi:10.1038/nmeth.3543
- Morita, S. and Terada, T. (2014). Molecular mechanisms for biliary phospholipid and drug efflux mediated by ABCB4 and bile salts. *BioMed Res. Int.* 2014, 1-11. doi:10.1155/2014/954781
- Nakanishi, N. and Martindale, M. Q. (2018). CRISPR knockouts reveal an endogenous role for ancient neuropeptides in regulating developmental timing in a sea anemone. *eLife* 7, e39742. doi:10.7554/eLife.39742
- Neudeck, B. L., Loeb, J. M., Faith, N. G. and Czuprynski, C. J. (2004). Intestinal P Glycoprotein acts as a natural defense mechanism against listeria monocytogenes. *Infect. Immun.* 72, 3849-3854. doi:10.1128/IAI.72.7.3849-3854.2004
- Nicklisch, S. C. T., Rees, S. D., Mcgrath, A. P., Gökirmak, T., Bonito, L. T., Vermeer, L. M., Cregger, C., Loewen, G., Sandin, S., Chang, G. et al. (2016). Global marine pollutants inhibit P-glycoprotein: Environmental levels, inhibitory effects, and cocrystal structure. *Sci. Adv.* 2, e1600001. doi:10.1126/sciadv. 1600001
- Nigam, S. K. (2015). What do drug transporters really do? *Nat. Rev. Drug Discov.* **14**, 29-44. doi:10.1038/nrd4461
- Nottage, A. S. and Birkbeck, T. H. (1986). Toxicity to marine bivalves of culture supernatant fluids of the bivalve-pathogenic Vibrio strain NCMB 1338 and other marine vibrios. J. Fish Dis. 9, 249-256. doi:10.1111/j.1365-2761.1986.tb01009.x
- Nymark, M., Sharma, A., Hafskjold, M., Sparstad, T., Bones, A. and Winge, P. (2017). CRISPR/Cas9 gene editing in the marine diatom Phaeodactylum tricornutum. *Bio-Protocol* 7. doi:10.21769/BioProtoc.2442
- Ota, S., Hisano, Y., Ikawa, Y. and Kawahara, A. (2014). Multiple genome modifications by the CRISPR/Cas9 system in zebrafish. *Genes Cells* 19, 555-564. doi:10.1111/gtc.12154
- Panwala, C. M., Jones, J. C. and Viney, J. L. (1998). A novel model of inflammatory bowel disease: mice deficient for the multiple drug resistance gene, mdr1a, spontaneously develop colitis. *J. Immunol.* 161, 5733-5744.
- Piel, J. (2009). Metabolites from symbiotic bacteria. Nat. Prod. Rep. 26, 338-362. doi:10.1039/B703499G
- Pohnert, G. and Boland, W., Luis, E., Lin, Z., Jeet, S., Lesch, J., Hackney, J., Kim, J., Zhou, M. and Lai, J. et al. (2002). The oxylipin chemistry of attraction and defense in brown algae and diatoms. *Nat. Prod. Rep.* **19**, 108-122. doi:10.1039/s8068880
- Ramirez-Carrozzi, V. A., Sambandam E., Luis, Z., Lin, S., Jeet, J., Lesch, J., Hackney, J., Kim, M., Zhou, J., Lai et al. (2011). IL-17C regulates the innate immune function of epithelial cells in an autocrine manner. *Nat. Immunol.*, 12, 1159-1166. doi:10.1038/ni.2156
- Razali, N. M. and Wah, Y. B. (2011). Power comparisons of Shapiro-Wilk, Kolmogorov–Smirnov, Lilliefors and Anderson-Darling tests. J. Stat. Model. Anal. 22, 21-33.
- Ren, X., Yang, Z., Xu, J., Sun, J., Mao, D., Hu, Y., Yang, S.-J., Qiao, H.-H., Wang, X., Hu, Q. et al. (2014). Enhanced specificity and efficiency of the CRISPR/Cas9 system with optimized sgRNA parameters in Drosophila. *Cell Rep.* 9, 1151-1162. doi:10.1016/j.celrep.2014.09.044
- Rosenthal, S. B., Bush, K. T. and Nigam, S. K. (2019). A network of SLC and ABC transporter and DME genes involved in remote sensing and signaling in the gutliver-kidney axis. *Sci. Rep.* **9**, 11879. doi:10.1038/s41598-019-47798-x
- Schindelin, J., Arganda-Carreras, I., Frise, E., Kaynig, V., Longair, M., Pietzsch, T., Preibisch, S., Rueden, C., Saalfeld, S., Schmid, B. et al. (2012). Fiji: an open-source platform for biological-image analysis. *Nat. Methods* 9, 676-682. doi:10.1038/nmeth.2019
- Schinkel, A. H., Smit, J. J. M., Van Tellingen, O., Beijnen, J. H., Wagenaar, E., van Deemter, L., Mol, C. A. A. M., van der Valk, M. A., Robanus-Maandag, E. C., Te Riele, H. P. J. et al. (1994). Disruption of the mouse mdr1a P-glycoprotein gene leads to a deficiency in the blood-brain barrier and to increased sensitivity to drugs. *Cell* 77, 491-502. doi:10.1016/0092-8674(94)90212-7
- Schuh, N. W., Carrier, T. J., Schrankel, C. S., Reitzel, A. M., Heyland, A. and Rast, J. P. (2020). Bacterial exposure mediates developmental plasticity and resistance to lethal vibrio lentus infection in purple sea urchin (Strongylocentrotus purpuratus) Larvae. Front. Immunol. 10, 3014. doi:10.3389/fimmu.2019.03014
- Shevidi, S., Uchida, A., Schudrowitz, N., Wessel, G. M. and Yajima, M. (2017). Single nucleotide editing without DNA cleavage using CRISPR/Cas9-deaminase in the sea urchin embryo. *Dev. Dyn.*, 246, 1036-1046. doi:10.1002/dvdy.24586

- Shi, B., Xiang, X., Ke, Y., Zhou, L. and Ke, C. (2015). Abcb1 gene expression pattern and function of copper detoxification in Fujian oyster, Crassostrea angulata. Comp. Biochem. Physiol. B Biochem. Mol. Biol. 190, 8-15. doi:10.1016/ j.cbpb.2015.08.007
- Shipp, L. E. and Hamdoun, A. (2012). ATP-binding cassette (ABC) transporter expression and localization in sea urchin development. *Dev. Dyn.* 241, 1111-1124. doi:10.1002/dvdy.23786
- Siccardi, D., Mumy, K. L., Wall, D. M., Bien, J. D. and Mccormick, B. A. (2008).
 Salmonella enterica serovar Typhimurium modulates P-glycoprotein in the intestinal epithelium. Am. J. Physiol. Gastrointest. Liver Physiol. 294, G1392-G1400. doi:10.1152/ajpgi.00599.2007
- Smith, A. J., Van Helvoort, A., van Meer, G., Szabó, K., Welker, E., Szakács, G., Váradi, A., Sarkadi, B. and Borst, P. (2000). MDR3 P-glycoprotein, a phosphatidylcholine translocase, transports several cytotoxic drugs and directly interacts with drugs as judged by interference with nucleotide trapping. J. Biol. Chem., 275, 23530-23539. doi:10.1074/jbc.M909002199
- Smith, T. E., Pond, C. D., Pierce, E., Harmer, Z. P., Kwan, J., Zachariah, M. M., Harper, M. K., Wyche, T. P., Matainaho, T. K., Bugni, T. S. et al. (2018). Accessing chemical diversity from the uncultivated symbionts of small marine animals. *Nat. Chem. Biol.* 14, 179-185. doi:10.1038/nchembio.2537
- Song, X., Zhu, S., Shi, P., Liu, Y., Shi, Y., Levin, S. D. and Qian, Y. (2011). IL-17RE is the functional receptor for IL-17C and mediates mucosal immunity to infection with intestinal pathogens. *Nat. Immunol.* 12, 1151-1158. doi:10.1038/ni.2155
- Square, T., Romasek, M., Jandzik, D., Cattell, M. V., Klymkowsky, M. and Medeiros, D. M., (2015). CRISPR/Cas9-mediated mutagenesis in the sea lamprey Petromyzon marinus: a powerful tool for understanding ancestral gene functions in vertebrates. *Development* 142, 4180-4187. doi:10.1242/dev.125609
- Srikant, S., Gaudet, R. and Murray, A. W. (2020). Selecting for altered substrate specificity reveals the evolutionary flexibility of ATP-binding cassette transporters. *Curr. Biol.* 30, 1689-1702.e6. doi:10.1016/j.cub.2020.02.077
- Steele, J. A., Countway, P. D., Xia, L., Vigil, P. D., Beman, J. M., Kim, D. Y., Chow, C.-E. T., Sachdeva, R., Jones, A. C., Schwalbach, M. S. et al. (2011). Marine bacterial, archaeal and protistan association networks reveal ecological linkages. ISME J. 5, 1414-1425. doi:10.1038/ismej.2011.24
- Stumpp, M., Petersen, I., Thoben, F., Yan, J.-J., Leippe, M. and Hu, M. Y. (2020). Alkaline guts contribute to immunity during exposure to acidified seawater in the sea urchin larva. *J. Exp. Biol.* **223**, jeb222844. doi:10.1242/jeb.222844
- Su, L., Cheng, C. Y. and Mruk, D. D. (2009). Drug transporter, P-glycoprotein (MDR1), is an integrated component of the mammalian blood-testis barrier. Int. J. Biochem. Cell Biol., 41, 2578-2587. doi:10.1016/j.biocel.2009.08.015
- Su, L., Mruk, D. D., Lui, W.-Y., Lee, W. M. and Cheng, C. Y. (2011). P-glycoprotein regulates blood-testis barrier dynamics via its effects on the occludin/zonula occludens 1 (ZO-1) protein complex mediated by focal adhesion kinase (FAK). Proc. Natl Acad. Sci. USA, 108, 19623-19628. doi:10.1073/pnas.1111414108
- Szakács, G., Paterson, J. K., Ludwig, J. A., Booth-Genthe, C. and Gottesman, M. M., (2006). Targeting multidrug resistance in cancer. *Nat. Rev. Drug Discovery* 5, 219-234. doi:10.1038/nrd1984
- **Teuten, E. L.** (2005). Two abundant bioaccumulated halogenated compounds are natural products. *Science* **307**, 917-920. doi:10.1126/science.1106882
- Thomas, H. R., Percival, S. M., Yoder, B. K. and Parant, J. M. (2014). High-throughput genome editing and phenotyping facilitated by high resolution melting curve analysis. *PLoS ONE* 9, e114632. doi:10.1371/journal.pone.0114632

- Thompson, L. R., Sanders, J. G., Mcdonald, D., Amir, A., Ladau, J., Locey, K. J., Prill, R. J., Tripathi, A., Gibbons, S. M., Ackermann, G. et al. (2017). A communal catalogue reveals Earth's multiscale microbial diversity. *Nature*, 551, 457-463. doi:10.1038/nature24621
- **Toomey, B. H. and Epel, D.** (1993). Multixenobiotic resistance in urechis caupo embryos: protection from environmental toxins. *Biol. Bull.*, **185**, 355-364. doi:10. 2307/1542476
- Toomey, B. H., Kaufman, M. R. and Epel, D. (1996). Marine bacteria produce compounds that modulate multixenobiotic transport activity in Urechis caupo embryos. *Mar. Environ. Res.*, 42, 393-397. doi:10.1016/0141-1136(96)87094-2
- Tu, Q., Cameron, R. A. and Davidson, E. H. (2014). Quantitative developmental transcriptomes of the sea urchin Strongylocentrotus purpuratus. *Dev. Biol. Elsev.* 385, 160-167. doi:10.1016/j.ydbio.2013.11.019
- Turner, J. T. and Tester, P. A. (1997). Toxic marine phytoplankton, zooplankton grazers, and pelagic food webs. *Limnol. Oceanogr.* **42**, 1203-1213. doi:10.4319/lo.1997.42.5_part_2.1203
- Walworth, N. G., Zakem, E. J., Dunne, J. P., Collins, S. and Levine, N. M., (2020). Microbial evolutionary strategies in a dynamic ocean. *Proc. Natl Acad. Sci. USA*, 117, 5943-5948. doi:10.1073/pnas.1919332117
- Wessel, G. M., Kiyomoto, M., Shen, T.-L. and Yajima, M. (2020). Genetic manipulation of the pigment pathway in a sea urchin reveals distinct lineage commitment prior to metamorphosis in the bilateral to radial body plan transition. *Sci. Rep.* **10**, 1973. doi:10.1038/s41598-020-58584-5
- Whitehead, A., Pilcher, W., Champlin, D. and Nacci, D., (2012). Common mechanism underlies repeated evolution of extreme pollution tolerance. *Proc. R. Soc. B* **279**, 427-433. doi:10.1098/rspb.2011.0847
- Whitehead, A., Clark, B. W., Reid, N. M., Hahn, M. E. and Nacci, D. (2017). When evolution is the solution to pollution: Key principles, and lessons from rapid repeated adaptation of killifish (Fundulus heteroclitus) populations. *Evol. Appl.* 10, 762-783. doi:10.1111/eva.12470
- Wilson, M. C., Mori, T., Rückert, C., Uria, A. R., Helf, M. J., Takada, K., Gernert, C., Steffens, U. A. E., Heycke, N., Schmitt, S. et al. (2014). An environmental bacterial taxon with a large and distinct metabolic repertoire. *Nature*, **506**, 58-62. doi:10.1038/nature12959
- Wong, N., Liu, W. and Wang, X. (2015). WU-CRISPR: characteristics of functional guide RNAs for the CRISPR/Cas9 system. *Genome Biol.* 16, 218. doi:10.1186/ s13059-015-0784-0
- Xu, H., Xiao, T., Chen, C.-H., Li, W., Meyer, C. A., Wu, Q., Wu, D., Cong, L., Zhang, F., Liu, J. S. et al. (2015). Sequence determinants of improved CRISPR sgRNA design. Genome Res. 25, 1147-1157. doi:10.1101/gr.191452.115
- Yaguchi, S., Yaguchi, J., Suzuki, H., Kinjo, S., Kiyomoto, M., Ikeo, K. and Yamamoto, T. (2020). Establishment of homozygous knock-out sea urchins. *Curr. Biol.* **30**, R427-R429. doi:10.1016/j.cub.2020.03.057
- Yang, Q., Han, Y. and Zhang, X.-H. (2011). Detection of quorum sensing signal molecules in the family Vibrionaceae. *J. Appl. Microbiol.* 110, 1438-1448. doi:10. 1111/j.1365-2672.2011.04998.x
- Ying, Z. and Beronja, S. (2020). Embryonic barcoding of equipotent mammary progenitors functionally identifies breast cancer drivers. *Cell Stem Cell* 26, 403-419.e4. doi:10.1016/j.stem.2020.01.009
- Zhang, J.-H., Adikaram, P., Pandey, M., Genis, A., Simonds, W. F. (2016).

 Optimization of genome editing through CRISPR-Cas9 engineering.

 Bioengineered 7(3), 166-174. doi:10.1080/21655979.2016.1189039

Supplemental Figures

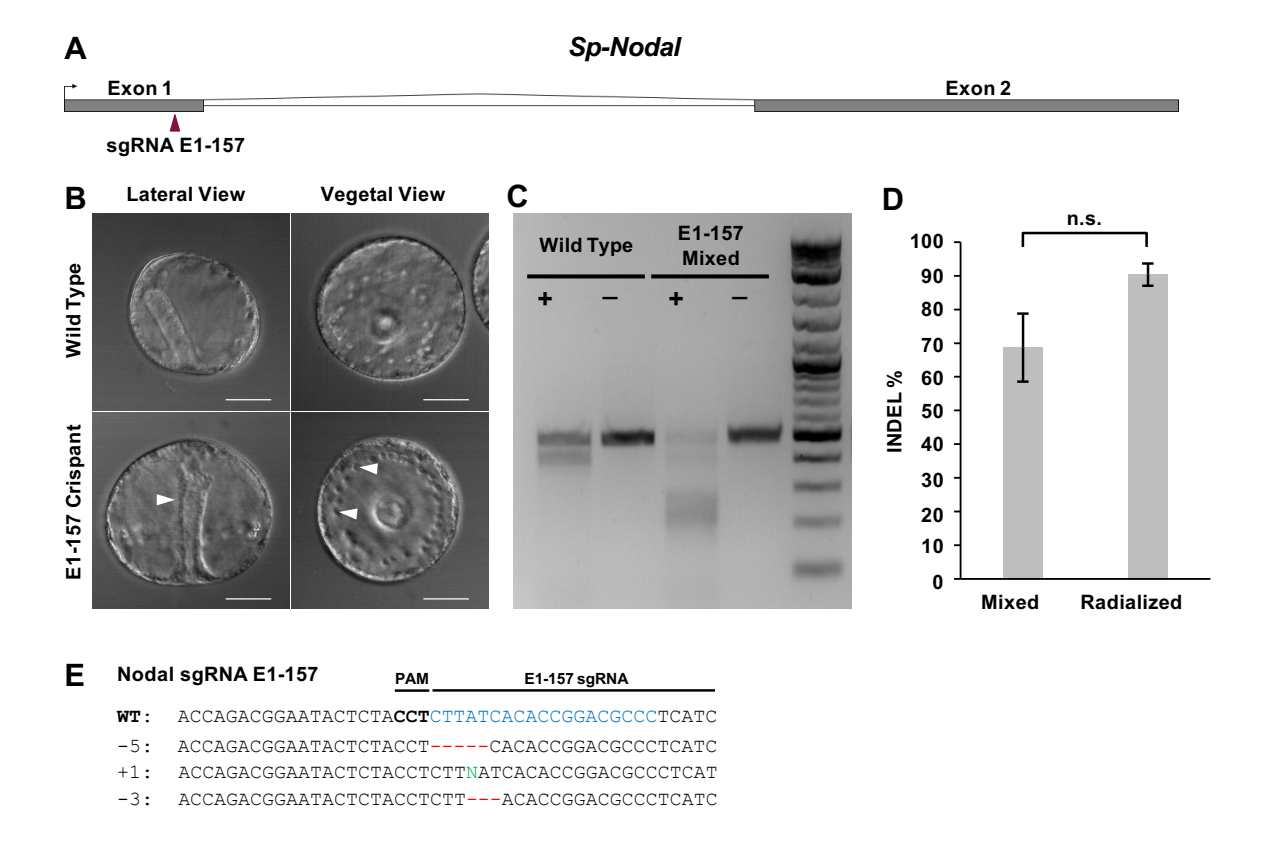


Figure S1. CRISPR/Cas9 mutagenesis efficiency in Sp-nodal sgRNA E1-157 crispants. (A)

Gene structure of *Sp-Nodal*. Red arrowhead indicates the synthetic sgRNAEx1-157 target site. **(B)** Lateral and vegetal views of WT and Nodal E1-157 Crispants. White arrowheads indicate the Nodal E1-157 crispant archenteron lack of bending toward the embryos' ventral side (left panels) and the altered position of primary mesenchyme cells (PMCs) (right panels). These characteristics are indicative of a radialized embryo. **(C)** T7EI assay of the PCR-amplified *Sp-Nodal*. Products were run on a 2% agarose gel. (+) represents T7EI-positive and (-) represents T7EI-negative reactions. **(D)** ICE analysis of CRISPR efficiency. Indel percentages are shown, (n = 4 batches). 'Mixed' and 'Radialized' correspond to ICE analyses of PCR amplicons from all injected embryos (a mix of WT-like and radialized embryos) and only injected embryos exhibiting the radialized phenotype, respectively. **(E)** ICE-predicted indels. ICE accurately predicts the identity and distribution of mutant alleles across populations of edited cells. The top

sequence for *Sp-Nodal* shows the wild type allele annotated to show the PAM site (bold) and sgRNA target sequence (blue text). The numbers on the left indicate the corresponding indel size for each mutant allele. Scale bars = $50 \, \mu M$.

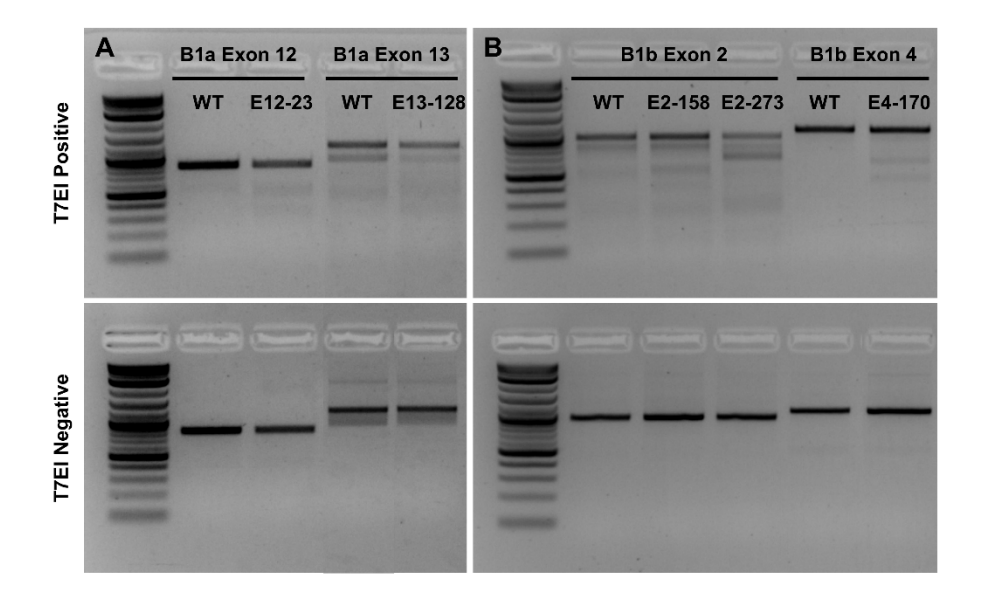


Figure S2. T7E1 assays of inefficient sgRNAs targeting *Sp-ABCB1a* and *Sp-ABCB1b*. T7EI assays of PCR-amplified regions of the sgRNA target sites for *Sp-ABCB1a* (**A**) and *Sp-ABCB1b* (**B**). Top panels show products incubated with T7E1. Bottom panels show denatured and reannealed heteroduplexes without the addition of T7E1.

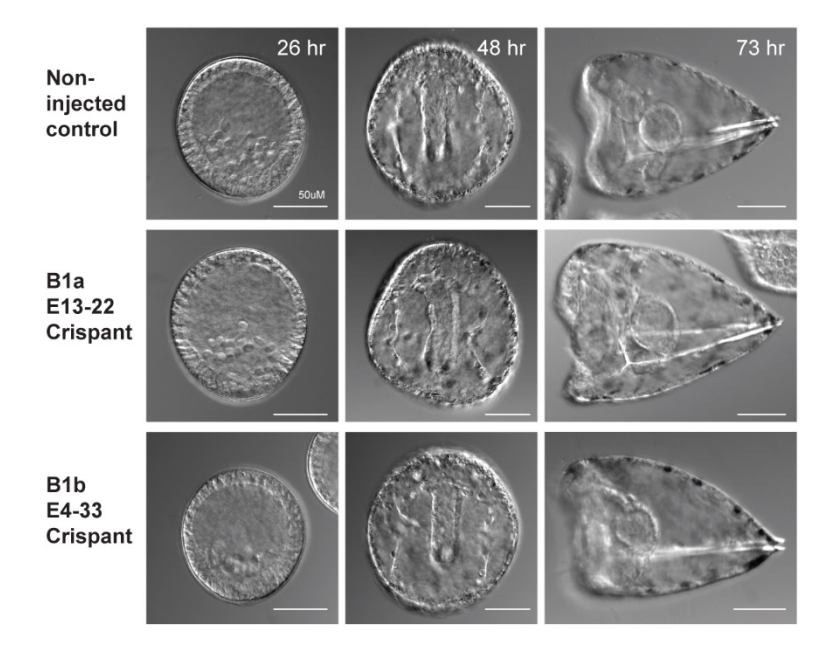


Figure S3. *Sp-ABCB1a* crispants exhibit normal development. Crispant and control embryos imaged at mesenchyme blastula (24-26 hr), gastrula (48 hr) and larval (73 hr) stages. Embryos did not exhibit morphological or developmental timing phenotypes (n=20 for each time point and condition). Representative DIC images are shown from one of two independent mate pairs. Scale bars = $50 \mu M$.

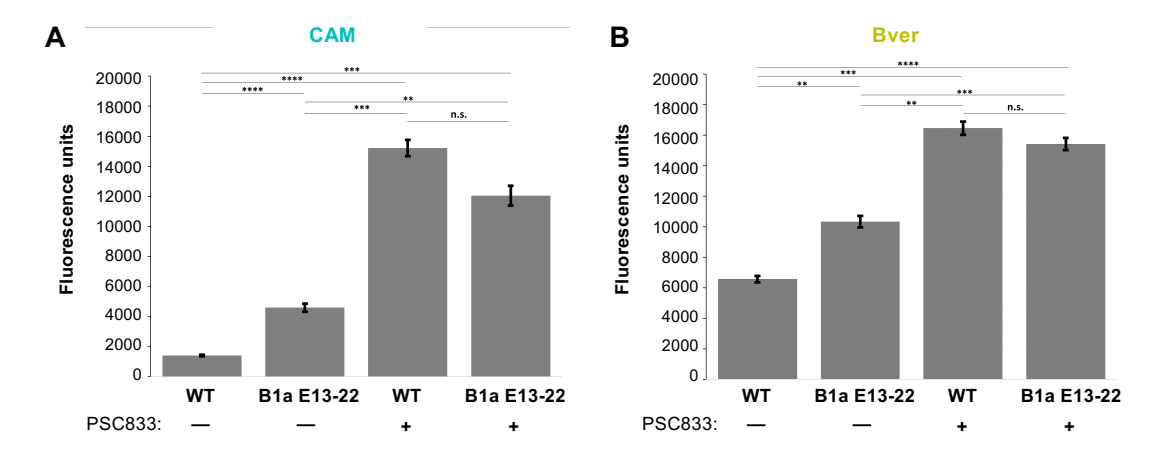


Figure S4. Bver and CAM accumulation in *Sp-ABCB1a* **crispants.** Bar graphs representing raw mean fluorescence values for Bver (A) and CAM (B) accumulation in control (WT) and B1aE13-22 crispants with and without 1 μ M PSC833 inhibitor. n=30-40 embryos from 3-4 biological repeats. **, P<0.01; ***, P<0.001; ****, P<0.0001; n.s., non-significant P>0.01.

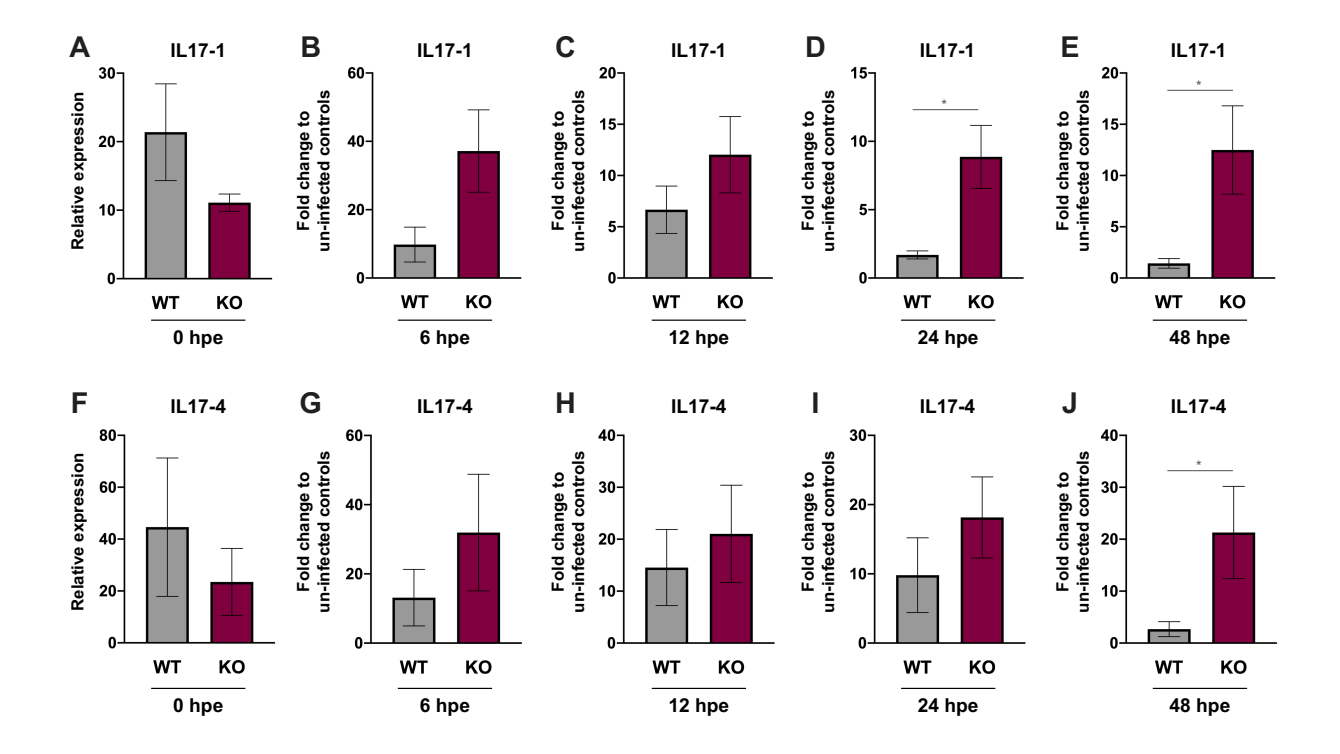


Figure S5. Changes in *Sp-IL-17* **expression between ABCB1 crispants and control (WT) larvae during** *Vibrio diazotrophicus* **infection.** Transcript prevalence was measured using qPCR. Expression values were normalized to 18S rRNA. Bar graphs representing relative expression at 0 hpe (**A, F**) and the fold-change in expression compared to un-infected 0 hpe larvae for *Sp-IL-17-1* (**B-E**) and *Sp-IL-17-4* (**G-J**). Crispant *Sp-IL-17* expression trends higher than control WTs at most timepoints and is significantly different at 24 and 48 hpe for *Sp-IL-17-1* (**D**, **P*=0.0262. **E**, **P*=0.0500) and 48 hpe for *Sp-IL-17-4* (**J**, **P*=0.0411). Unpaired t-tests with Welch's correction (**A, D, E**) or Mann-Whitney tests (**B, C, F-J**). n=6 internal replicates pooled from three biological replicates.

Supplemental Tables

Table S1. Primers and MASO sequences used for genomic PCR amplification of target loci, *in-situ* hybridization probe cloning, quantitative PCR, and antisense knockdown.

Gene locus	Forward primers (5'-3')	Reverse primers (5'-3')
Sp-Nodal Ex1 for both T7EI and ICE	CTGAGACATCCCAGTGACGA	TGATTTACCCACACAGCA
Sp-ABCB1a Ex12 for T7EI	GCAGCTGAAGAGAAAGCTCAAATAA	CGAGAAAGGGACATACAGACG
Sp-ABCB1a Ex12 for ICE	TTTAGGTGACACTATAG TGTAAAACGA CGGCCAGTGCAGCTGAAGAGAAAGCTC AAATAA	TAATACGACTCACTATAGGGAGGAAACAGCT ATGACCGAGAAAGGGACATACAGACG
Sp-ABCB1a Ex13 for T7EI	CAGGTGGTTATCTCATCAAATCAG	GTCAGAGTTGAAGATGGTTGAGAGAC
Sp-ABCB1a Ex13 for ICE	ATTTAGGTGACACTATAGTGTAAAACG ACGGCCAGTCAGGTGGTTATCTCATCA AATCAG	TAATACGACTCACTATAGGGCAGGAAACAGC TATGACTACAGTTGGAAAAGCTGGGAAAA
Sp-ABCB1b Ex2 for T7EI	TTTCATGCCCGGGATTTTATGTTCACC	GTCGGTTTAGTTCAAATTTAGACCTTGCAG
Sp-ABCB1b Ex4 for T7EI	GGTACAGTTGAATTCTTGACGTGTGAT	GTACTAATCATTCATCTAGGCCCATTG
Sp-ABCB1b Ex4 for ICE	TTTAGGTGACACTATAG TGTAAAACGA CGGCCAGTAGTAATCTTGCTGAAAACT GCACAC	GACTCACTATAGGGCAGGAAACAGCTATGAC GTACTAATCATTCATCTAGGCCCATTG
Sp-ABCB1a ISH Antisense probe cloning	CCCACCTGCTGTGGGTTTCTCCAAT	AAGTAATACGACTCACTATAGGGAGAGCCCG CATCCACTGCTGCCAACCATG
Sp-ABCB1a ISH Sense probe cloning	AAGTAATACGACTCACTATAGGGAGAG CCCACCTGCTGTGGGTTTCTCCAAT	CCCGCATCCACTGCTGCCAACCATG
Sp-18S qPCR	CAGGGTTCGATTCCGTAGAG	CCTCCAGTGGATCCTCGTTA
Sp-IL17-1 qPCR	CATCAAGCTGCCCATACGAT	GCTGATCGACATCGGGATAC
Sp-IL17-4 qPCR	CTCTGTCCCAGGAAGCAATA	GGTGGCCAGTGGGTCTTC
Control MASO	CCTCTTACCTCAGTTACAATTTATA	
Sp-ABCB1a MASO	TCTCTTTATCTTGGAGGCCAGGC	

Forward primers used to prepare amplicons for Sanger sequencing/ICE are 60mers containing part of the SP6 promoter sequence, **M13 forward sequence** and the corresponding <u>gene-specific primer</u> sequence used for amplification for T7E1 assays. Reverse primers are similarly designed but the SP6 promoter sequence is replaced with a portion of the T7 promoter.